

Fall 1998

## Fatigue Life Prediction of Edge-Welded Metal Bellows Using Neural Networks and Multiple Linear Regression

David L.W. Ballard

*Embry-Riddle Aeronautical University - Daytona Beach*

Follow this and additional works at: <https://commons.erau.edu/db-theses>



Part of the [Aerospace Engineering Commons](#)

---

### Scholarly Commons Citation

Ballard, David L.W., "Fatigue Life Prediction of Edge-Welded Metal Bellows Using Neural Networks and Multiple Linear Regression" (1998). *Theses - Daytona Beach*. 14.

<https://commons.erau.edu/db-theses/14>

This thesis is brought to you for free and open access by Embry-Riddle Aeronautical University – Daytona Beach at ERAU Scholarly Commons. It has been accepted for inclusion in the Theses - Daytona Beach collection by an authorized administrator of ERAU Scholarly Commons. For more information, please contact [commons@erau.edu](mailto:commons@erau.edu).

# **Fatigue Life Prediction of Edge-Welded Metal Bellows Using Neural Networks and Multiple Linear Regression**

by

David L.W. Ballard

A Thesis Submitted to the Graduate Studies Office  
in Partial Fulfillment of the Requirements for the Degree of  
Master of Science in Aerospace Engineering

Embry-Riddle Aeronautical University  
Daytona Beach, Florida  
Fall 1998

UMI Number: EP31815

### INFORMATION TO USERS

The quality of this reproduction is dependent upon the quality of the copy submitted. Broken or indistinct print, colored or poor quality illustrations and photographs, print bleed-through, substandard margins, and improper alignment can adversely affect reproduction.

In the unlikely event that the author did not send a complete manuscript and there are missing pages, these will be noted. Also, if unauthorized copyright material had to be removed, a note will indicate the deletion.

**UMI**<sup>®</sup>

---

UMI Microform EP31815  
Copyright 2011 by ProQuest LLC  
All rights reserved. This microform edition is protected against  
unauthorized copying under Title 17, United States Code.

---

ProQuest LLC  
789 East Eisenhower Parkway  
P.O. Box 1346  
Ann Arbor, MI 48106-1346

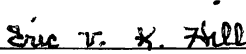
# Fatigue Life Prediction of Edge-Welded Metal Bellows Using Neural Networks and Multiple Linear Regression


by

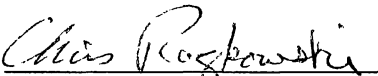
David L.W. Ballard

This thesis was prepared under the direction of the candidate's thesis committee chairman, Dr. Eric v. K. Hill, Department of Aerospace Engineering, and has been approved by the members of his thesis committee. It was submitted to the Department of Aerospace Engineering and was accepted in partial fulfillment of the requirements for the degree of Master of Science in Aerospace Engineering.

## THESIS COMMITTEE

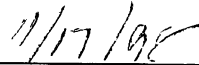
  
\_\_\_\_\_  
Dr. Eric v. K. Hill  
Chairman

  
\_\_\_\_\_  
Dr. Deborah M. Osborne  
Member

  
\_\_\_\_\_  
Mr. Christopher J. Raczowski  
Member

  
\_\_\_\_\_  
Graduate Program Coordinator, MSAE

  
\_\_\_\_\_  
Department Chair, Aerospace Engineering

  
\_\_\_\_\_  
Date

## ACKNOWLEDGMENTS

I would like to thank, above all others, my parents who encouraged and helped to support me throughout my college career. I would like to thank Dr. Eric v. K. Hill, my thesis advisor, who's enthusiasm and unique style of motivation resulted in my accomplishing a level of work exceeding my expectations. His teaching direction and insight have focused my professional direction more within my two years of graduate school than that which I achieved during my working career and years of undergraduate study. I would also like to thank the members of my thesis committee, Dr. Deborah M. Osborne and Christopher J. Raczkowski, who helped me in accomplishing my education and research goals. A special thanks to those who made this research possible: Christopher J. Raczkowski at EG&G Belfab, without his support and direction this project would still be a proposal on paper; fellow graduate student Jeffery B. Allen, without his analysis and statistical help I would not have been able to attain a more thorough level of research; EG&G Belfab, for financially backing this research and offering the use of manufacturing and testing facilities; and all employees of EG&G Belfab who offered their labor and expertise.

Author : David L. W. Ballard  
Title : Fatigue Life Prediction of Edge-Welded Metal Bellows Using Neural Networks and Multiple Linear Regression  
Institution : Embry-Riddle Aeronautical University  
Degree : Master of Science in Aerospace Engineering  
Year : 1998

## ABSTRACT

Edge-welded metal bellows present an ongoing challenge: the prediction of an accurate cycle life. Current methods rely on physical leak detection to determine a bellow's cycle life to failure. It is known, however, that crack initiation begins many cycles before a leak path is present. Bellows manufacturers require a method for detection of fatigue cracks when they initiate but before they result in leak rates large enough to contaminate a process. Acoustic emission (AE) testing is one method which can meet this need and is a proven, reliable technique for detecting crack initiation and monitoring fatigue crack growth.

Four sets of metal bellows samples were fatigue tested and AE parameter data recorded. The data sets were analyzed and the determination made that amplitude, duration, and time of occurrence were the AE data variables required for separation of the various failure mechanisms.

For two of the four materials, an expanded set of tests were performed. Fourteen tests were used to train and test a back-propagation neural network for prediction of bellows cycle life. The input data consisted of a material identifier, AE parameter data consisting of the amplitude distribution (50-100 dB) of the first 250 hits, and the final cycle life. The network was structured with an input layer consisting of the identifier and amplitude data, two hidden layers for mapping failure mechanisms, and an output layer for predicting cycle life. The network required training on four samples for the Inconel 718 and five samples for the 350 stainless steel. Once trained the network was able to predict cycle life with a worst case error of -4.45 percent and 2.66 percent for the Inconel 718 and 350 stainless steel, respectively.

Finally, through the use of multiple linear regression, a statistical analysis was made to develop a model capable of accurate prediction. Applying a natural log transformation to the independent variables of amplitude and energy resulted in a model capable of explaining 95 percent of the variability in cycle life prediction.

# TABLE OF CONTENTS

	Page
Signature Page	ii
Acknowledgments	iii
Abstract	iv
Table of Contents	v
List of Figures and Tables	vii
CHAPTER 1 - INTRODUCTION	1
1.1 Overview	1
1.2 Previous Research	2
1.3 Current Research	2
CHAPTER 2 - BACKGROUND THEORY	3
2.1 Acoustic Emission	3
2.2 Neural Networks	5
2.3 Regression Methods	8
CHAPTER 3 - EQUIPMENT SET-UP AND TESTING	11
3.1 Equipment Set-up	11
3.1.1 Metal Bellows Seal	11
3.1.2 Final Assembly	11
3.1.3 AE Transducers and Preamplifiers	12
3.1.4 Pressurization	13
3.1.5 Data Acquisition	14
3.2 Testing Procedure	14
3.3 Data Processing	15
CHAPTER 4 - NEURAL NETWORKS	16
4.1 Back-propagation Network	16
4.2 Back-propagation Architecture	16
4.3 Back-propagation Algorithm	18
4.4 Back-propagation Example	19

	<b>Page</b>
<b>CHAPTER 5 - ANALYSIS AND RESULTS</b>	21
5.1 AE Data Analysis	21
5.2 Amplitude Distributions	24
5.3 Fatigue Analysis	26
5.4 Neural Network Results	31
5.5 Multiple Linear Regression Analysis	34
<b>CHAPTER 6 - CONCLUSIONS AND RECOMMENDATIONS</b>	40
6.1 Conclusions	40
6.1.1 Failure Mechanics	41
6.1.2 AE Parameter Data	41
6.1.3 Neural Networks and Multiple Linear Regression	42
6.2 Recommendations	43
<b>REFERENCES</b>	45
<b>BIBLIOGRAPHY</b>	46



## LIST OF FIGURES AND TABLES

Figure / Table		Page
Figure 2.1	Resonant transducer for detection of acoustic emission activity	3
Figure 2.2	AE transducer receiving, converting, and transmitting energy waves to the data acquisition system	4
Figure 2.3	Typical waveform depicting measured AE parameters	5
Figure 2.4	An artificial neuron with a hyperbolic tangent activation function	6
Figure 2.5	Hyperbolic tangent sigmoid function with translation term $\theta$	7
Figure 3.1	Typical metal bellows test specimen	11
Figure 3.2	Final assembly set-up	12
Figure 3.3	Testbed components and set-up configuration	13
Figure 4.1	Back-propagation neural network used for predicting cycle life	17
Figure 5.1	Duration versus amplitude plot with crack initiations, Region I events	22
Figure 5.2	Duration versus amplitude plot with stable crack propagations, Region II events	22
Figure 5.3	Duration versus amplitude plot with rapid crack growth, Region III events	23
Figure 5.4	Duration versus amplitude plot with vacuum evacuation.	23
Figure 5.5	350 stainless steel cumulative hits versus amplitude histogram plot with defined failure mechanism “humps”	25
Figure 5.6	Inconel 718 nickel alloy cumulative hits versus amplitude histogram plot with defined failure mechanism “humps”	25
Figure 5.7	Stress distribution at I.D. weld during stroke at maximum extension	27
Figure 5.8	Stress distribution at I.D. weld during stroke at maximum compression	28
Figure 5.9	Typical HAZ region failures for Inconel 718 nickel alloy	29
Figure 5.10	Typical HAZ region failures for 350 stainless steel	29
Table 5.1	Failure locations for each test specimen with reference to the dual flat adapter	30
Figure 5.11	Histogram of weld failure locations for all materials tested	31

<b>Figure / Table</b>		<b>Page</b>
<b>Table 5.2</b>	<b>Training and testing data for Inconel 718 and 350 stainless steel test specimens</b>	<b>32</b>
<b>Table 5.3</b>	<b>Neural network training and testing parameters</b>	<b>33</b>
<b>Table 5.4</b>	<b>Summary of the network testing results</b>	<b>33</b>
<b>Figure 5.12</b>	<b>Scatterplot matrix for comparison of AE parameters</b>	<b>34</b>
<b>Figure 5.13</b>	<b>Final scatterplot matrix for multiple linear regression analysis</b>	<b>35</b>
<b>Figure 5.14</b>	<b>Plot of studentized residuals versus predicted cycle life</b>	<b>37</b>
<b>Figure 5.15</b>	<b>Normal probability plot for studentized residuals</b>	<b>37</b>
<b>Figure 5.16</b>	<b>Plot of observed cycle life versus predicted cycle life</b>	<b>38</b>

# CHAPTER 1

## INTRODUCTION

### 1.1 OVERVIEW

In most cases, metal bellows experience failure as a result of cyclic or fatigue loads. Such loadings initiate the nucleation and propagation of cracks through a material, especially in high-strength, corrosion-resistant alloys similar to those investigated herein. Such alloys sometimes require a heat treatment process that offers a gain in strength but is offset by a reduction in ductility. A majority of metal bellows are comprised of these materials and are subjected to cyclic loadings; therefore, the onset of fatiguing is of importance. To identify and characterize the effects from these loads and material changes, the implementation of an acoustic emission monitoring system and neural network analysis has been proposed as an addition to the reliability testing methods presently used at EG&G Belfab. Currently, cyclic stroking of the bellows and physical leak detection are the methods for determining a bellows cycle life and failure. It is known, however, that crack initiation begins many cycles before a leak path is present. Therefore it was warranted to research and develop a method for detecting fatigue cracks when they initiate, but before they result in leak rates large enough to contaminate a process. AE is one method for detecting crack initiation and is a proven, reliable technique for monitoring fatigue crack growth.

To accurately predict cycle life an evaluation and some assumptions must be made on the recorded data. A determination must first be made as to which variables are likely to have the greatest impact on the desired output variable, in this case cycle life. Once a selection has been made, a prediction can be made on the variables through the use of neural network analysis. Tests incorporating filament wound composite pressure vessels have proven neural network analysis to be a reliable method for predicting burst pressures [Kalloo, 1998; Hill, 1992], while tests incorporating aluminum-lithium weld specimens have proven successful in predicting ultimate weld strength through the use of neural networks [Hill et al., 1993].

AE signal data sets have characteristics that many times can be used to identify failure mechanisms. Metals have various AE parameters that correspond to such mechanisms as plastic deformation or crack propagation. Within these categories can exist sub-categories

that are separable by the severity or length of the signal. A third mechanism of leakage was noted to exist after crack breakthrough as a result of internal vacuum release. Each of these failure mechanisms tends to generate a characteristic AE signal. Moreover, each mechanism contributes its effect to the integrity of the total structure in varying degrees. As a result each mechanism is weighted differently by the neural network according to the effect it has on the fatigue life. Plastic deformations tend to have weighting coefficients near zero while crack propagations have much higher values. Neural networks provide an automated technique for sorting out the AE associated with the various mechanisms and determining the appropriate coefficients or weighting functions [Sachse et. al., 1992] to predict a cycle life to failure for each tested sample.

## **1.2 PREVIOUS RESEARCH**

AE is a proven and commonly used method for weld monitoring. Unfortunately, no previous research has been found which incorporates both a tungsten/inert gas (TIG) welding and thin materials using sheet stocks less than 0.031 inch thick. The most applicable research to date focuses on structures constructed of plate or bar stocks which incorporate a TIG or arc welding process. Materials used in these tests are much thinner sheet stock, 0.004 inch thick, making the value of existing research questionable.

## **1.3 CURRENT RESEARCH**

The purpose of this research focused on two requirements: (1) to develop a method for identifying the occurrence and characteristics of specific fatigue modes for commonly used stainless steels and nickel-based alloys; and (2) to develop a method for predicting metal bellows cycle life. By supplying an applied load, in this case an extension/compression cycle and an internal vacuum pressure, the fatigue modes could be detected through the use of an acoustic emission monitoring system and categorized by evaluating AE parameter data. The recorded AE parameter data could then be developed for input into a neural network for cycle life prediction.

## CHAPTER 2

### BACKGROUND THEORY

#### 2.1 ACOUSTIC EMISSION

Acoustic emission is a noninvasive, passive technique for detecting fatigue in structures under load. Any material (metals, composites, wood, etc.) can be analyzed by this method. Its two greatest benefits over other nondestructive techniques are that a structure can be analyzed both globally and on a real time basis. Other nondestructive techniques such as eddy current, radiography, and ultrasonics allow for monitoring a small area of a structure at any one time. In many cases complex geometry can greatly reduce the test accuracy and extend the time required for testing, making these methods costly and/or ineffective. For AE this is not a problem since the waves generated by flaw growth activity propagate throughout the structure. AE is also advantageous in that a structure can be tested while in service, reducing costly down time. These advantages make AE the most plausible method for monitoring edge-welded metal bellows for fatigue crack detection.

Acoustic emission transducers (Figure 2.1) detect the stress waves emitted from sudden deformations within a material. Such deformations result in a rapid release of energy that propagates through the material until it dampens out or attenuates. Within the transducer is a piezoelectric element which acts as a receiver and transmitter. The energy wave is received by the transducer which in turn emits a voltage signal in response to the energy wave received. A couplant layer acts as a waveguide allowing the released energy waves to be detected by the transducer.

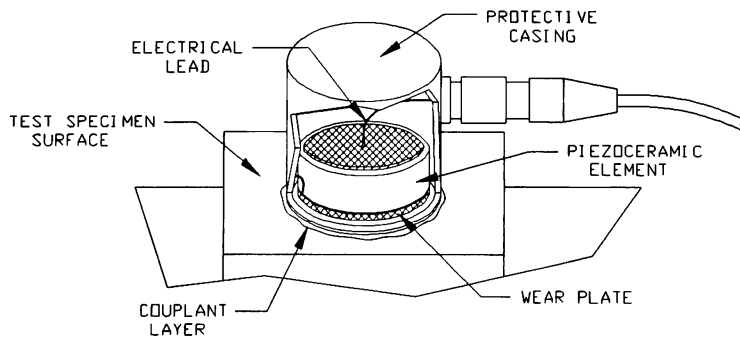


Figure 2.1. Resonant transducer for detection of acoustic emission activity.

The resulting voltage signal emitted by the transducer is transmitted to the data acquisition system where the signal is amplified and digitized. The waveforms and specified AE parameters are then recorded for each received signal. Figure 2.2 depicts an example of an AE transducer and data acquisition system used to detect cracking. As the crack propagates, it releases energy waves that are detected by the AE transducer. The received energy wave is then converted to an electrical signal by the transducer and sent to the data acquisition system where the signal is digitized and specified AE parameter data are extracted.

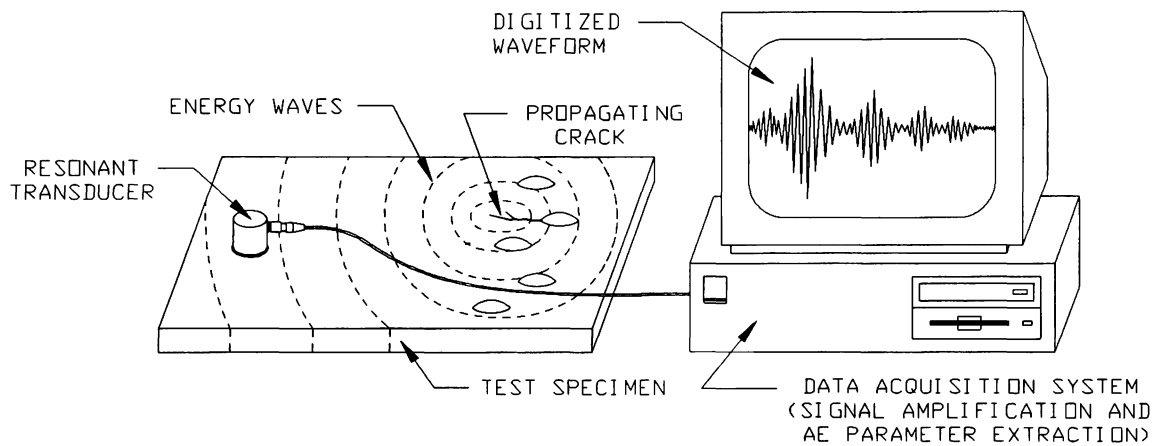


Figure 2.2. AE transducer receiving, converting, and transmitting energy waves to the data acquisition system.

Figure 2.3 represents a voltage versus time signal and the associated AE parameters as recorded by the data acquisition system. Amplitude is the peak voltage of the incoming signal expressed in decibels (dB). Counts is the number of times the voltage signal crosses a set threshold. By setting a high enough threshold, external sources of noise can be eliminated from the pertinent data. Setting a low threshold allows for smaller AE events to be detected. However, unless the environment is free of external noise sources, small AE events tend to be masked by higher amplitude sources. Counts-to-peak is the number of counts crossing a predetermined threshold before the signal reaches its maximum amplitude. Duration is the time in which the voltage signal exists above the set threshold. This is measured from the first time the signal crosses the threshold to the last time the signal falls below the threshold. Energy is the sum of all areas beneath the rectified voltage signal. Generally, the areas beneath the 0.0 volt line are inverted, or rectified, to represent a positive voltage that is

referred to as the Measured Area Under the Rectified Signal Envelope (MARSE). In Figure 2.3 this parameter is represented by the sum of all shaded areas bounded by the waveform and the 0.0 volt line. Finally, the risetime is the time it takes for the signal to reach its maximum amplitude.

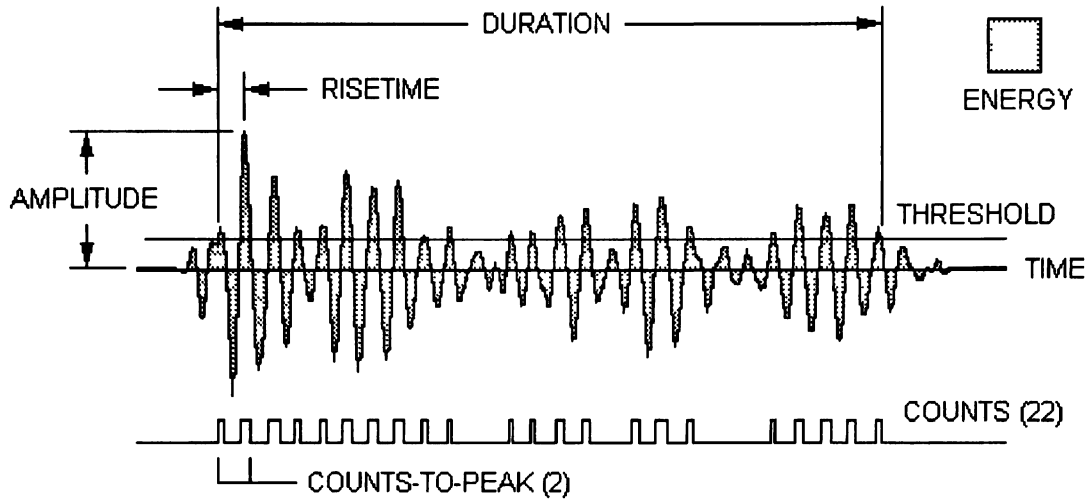


Figure 2.3 Typical waveform depicting measured AE parameters.

## 2.2 NEURAL NETWORKS

Neural networks are composed of numerous highly interconnected processing elements that work in parallel to solve a specific problem. Like the human brain, neural networks cannot be programmed to perform specified tasks but must learn by example prior to correctly processing information. A benefit of neural network learning is that sets of test data can be generalized and evaluated without initially identifying or isolating the relevant factors from the remaining test data. Regardless of extraneous data or the existence of data overlap, neural networks have an increased tolerance to noisy data and can work by learning all the pertinent data interactions for accurate prediction.

Normally, a neural network will have several layers consisting of a pre-determined number of neurons. A neuron is a component of an artificial neuron that consists of a continuous differential transfer function (generally a hyperbolic tangent, sigmoid function, or simple threshold function) which prevents its output magnitude from becoming so large that other neurons effectively become zero. The basic and most commonly used architecture of a

neural network consists of an input layer, a center or hidden layer, and an output layer. Connections exist between the neurons of adjacent layers to relay the output signal from one layer to the next. Fully connected networks occur when all nodes in each layer receive connections from all nodes in each preceding layer and are referred to as feed-forward networks.

Information is input to the network through each neuron of the input layer. The input layer neurons' specific function is to direct information to the processing or hidden layer. The hidden and output layers contain neurons that process all incoming data. All inputs to each neuron are weighted, combined, and processed through a transfer function that controls the signal magnitude relayed through the neuron's output connection.

An example of a simple neural network consists of a single artificial neuron (Figure 2.4). Within the artificial neuron exist weight vector components,  $w_i$ , and input vector components,  $x_i$ . Each input vector component is processed through and multiplied by its corresponding weight vector component. All resulting products are then summed up over all inputs to yield a NET output:

$$\text{NET} = \sum_i (w_i x_i) \tag{1}$$

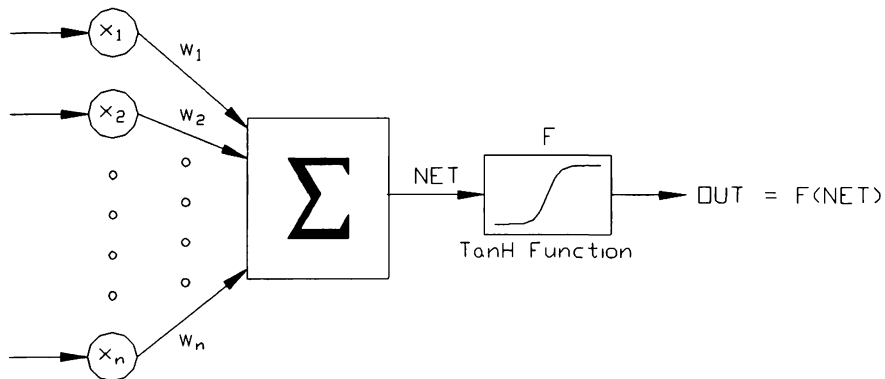


Figure 2.4. An artificial neuron with a hyperbolic tangent activation function.

In many cases each hidden and output layer is connected to an additional neuron called a bias. Bias neurons have a constant value of +1 but also have a weighted connection that trains like all other connection weights. Bias neurons improve the speed of training by simply outputting



a bias signal that applies a horizontal translation to the transfer function, resulting in a translation toward a more optimum (greater) slope within the sigmoid function. The translation term,  $\theta$ , is a factor added to or subtracted from the total input of a neuron and is included as follows:

$$\text{NET} = \theta + \sum_i (w_i x_i) \quad (2)$$

This model would suffice for modeling linear processes, but with nonlinear processes such as those encountered in this application, a nonlinear activation function,  $F$ , must be applied to the NET output. Here a nonlinear hyperbolic tangent activation function was employed as a squashing function:

$$\text{OUT} = F(\text{NET}) = [(e^{\text{NET}} - e^{-\text{NET}}) / (e^{\text{NET}} + e^{-\text{NET}})] \quad (3)$$

As NET approaches large positive values, OUT approaches a limiting value of +1; when NET equals 0, OUT equals 0; and when NET approaches large negative values, OUT approaches a limiting value of -1. Figure 2.5 represents a plot of this function along with the translation term  $\theta$ . Use of this transfer function serves to normalize data and provide a nonlinear gain to allow each neuron to process inputs with both large or small magnitudes without incurring problems with noise saturation [Wasserman, 1989].

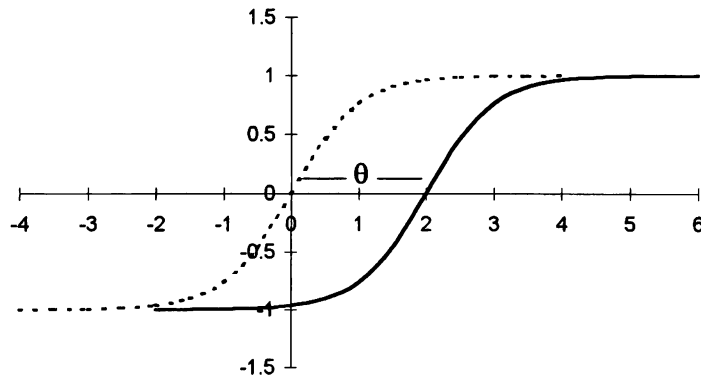


Figure 2.5. Hyperbolic tangent sigmoid function with translation term  $\theta$ .

Normally, networks containing multiple hidden layers will employ nonlinear activation functions throughout, so as to produce a nonlinear mapping result. Once a test data set has been applied and a state of optimization attained, the interconnection weights are saved to prevent further adjustments in the network structure. At this point the network is considered

to be “trained” and ready to make accurate predictions on various failure mechanisms using data sets comparable to those trained upon.

### 2.3 REGRESSION METHODS

There are considerable similarities between the theories of statistics and neural networks. Both are primarily concerned with data analysis. Data that can be generalized upon effectively by a neural network can usually be analyzed successfully using an appropriate statistical method. Regression is one such statistical method consisting of several types of analyses.

Linear regression is a statistical technique that models the relationship between an independent variable and a dependent variable by fitting a linear equation to a set of collected data. The independent variable  $x_1$  is associated with a value of the dependent variable  $Y | x_1$ . The population regression line for a single independent variable is defined as:

$$\mu_{Y | x_1} = \beta_0 + \beta_1 x_i + E_i \quad (4)$$

The estimated model, a result of sample data taken from a population, is an estimation of the regression line produced by the population and is defined as:

$$y = b_0 + b_1 x_1 + \varepsilon_i \quad (5)$$

The value  $E_i$  is a random error of the population model and must have a mean value of zero. Since the value  $\varepsilon_i$  is an estimation of the population model’s random error, a non-zero value will exist. However, with the random error,  $E_i$ , of the population line being unknown the expected value,  $\varepsilon_i$ , is assumed to be zero. To evaluate the effect of errors, an analysis of the resulting residuals (errors) can be made.

Using the method of least squares, the variables  $b_0$  and  $b_1$  (estimates for  $\beta_0$  and  $\beta_1$ ) can be found so that the sum of the squares of the residuals are minimized. The least squares estimates  $b_0$  and  $b_1$  are computed as:

$$b_0 = \bar{y} - b_1 \bar{x} \quad (6)$$

$$b_1 = [\Sigma(x_1 - \bar{x})(y_1 - \bar{y})] / \Sigma(x_1 - \bar{x})^2 \quad (7)$$

Multiple linear regression is a second statistical technique that models the relationship between two or more independent variables and a dependent variable by fitting an equation to a set of collected data. Generally, most applications of research data will contain complex mechanisms that require more than one independent variable in the regression model. For a set of  $k$  independent variables,  $x_1, x_2, \dots, x_k$ , the mean of the dependent variable  $Y | x_1, x_2, \dots, x_n$  is given by the population multiple linear regression model:

$$\mu_{Y | x_1, x_2, \dots, x_k} = \beta_0 + \beta_1 x_1 + \beta_2 x_2 + \dots + \beta_k x_k + E \quad (8)$$

The estimated model, a result of sample data taken from a population, is an estimation of the regression line produced by the population data and is defined as:

$$y = b_0 + b_1 x_1 + b_2 x_2 + \dots + b_k x_k + \varepsilon \quad (9)$$

For both methods, fitted values,  $b_i$ , are used as estimates of the parameters,  $\beta_i$ , of the population regression model. These predictor variables are computed by minimizing the sum of the squares of the vertical deviations from each data point to a fitted line. If a point lies on the fitted line, then the vertical deviation is zero. By first squaring then summing all deviations, cancellations between positive and negative values are alleviated.

In some cases, linear regression methods can result in poor predictions due to non-linearity existing between variables. To consider the effects of such non-linearities, a transformation may be applied to the data set. A regression model which contains transformed  $x$  and/or  $y$  variables does not result in the model becoming nonlinear. For example, if a logarithmic model is applied to Equation (5), the transformation occurs to the natural  $x$  variable.

$$y = a + b \log x_1 + \log \varepsilon \quad (10)$$

By letting  $x_1' = \log x$  and  $\varepsilon' = \log \varepsilon$ , the equation can be written as:

$$y = a + b x_1' + \varepsilon' \quad (11)$$

Although the model has become nonlinear in the  $x$  variable, it remains linear in the  $b$  parameter and can therefore be treated as linear [Walpole et. al., 1998].

An advantage of today's statistical software is the ability to quickly evaluate many models for a set of variables. By using an advanced regression option, it is possible to

examine all combinations of input variables as long as they are not linear combinations of other terms within the model. When a linear relationship exists between variables, only one of the terms is required in the model to reflect the contribution of all variables. With no linear combinations existing and setting the number of independent variables to  $k = 3$ , for simplicity, there exists nine possible terms:  $x_1$ ,  $x_2$ ,  $x_3$ ,  $x_1 x_2$ ,  $x_1 x_3$ ,  $x_2 x_3$ ,  $x_1^2$ ,  $x_2^2$ , and  $x_3^2$ . Therefore, for a dependent variable,  $y$ , the complete regression model is defined as:

$$y = b_0 + b_1 x_1^2 + b_2 x_2^2 + b_3 x_3^2 + b_4 x_1 x_2 + b_5 x_1 x_3 + b_6 x_2 x_3 + \varepsilon \quad (12)$$

It is unlikely that all variables will have a significant impact on the model. Therefore, an analysis of adjusted  $R^2$  values and p-values must be made to determine which model combination offers the greatest prediction ability. The adjusted  $R^2$  (sample coefficient of multiple determination) value is a measurement that explains the proportion of the total variation in the values of the variable  $y$  that can be explained by the regression model with the values of the random variables  $x_i$ . The p-value is a measure of the statistical significance of the model [Walpole et. al., 1998]. Generally, the simplest model with the highest adjusted  $R^2$  value and lowest p-value (less than 0.1) is considered to have the “best” predictive characteristics. Once a model combination has been selected, plots of the residuals, resulting from the calculated variable  $y$ , can be generated. These plots are important in that they will identify the scatter of error (a uniform scattering about the lines is desired), identify whether a linear “fit” of the data exists, and check for normality of the errors in the model. Cases can occur where model combinations show excellent predictability resulting in a high adjusted  $R^2$  value and a low p-value. However, when the statistics of the model is evaluated, it is discovered the model has been over-specified, resulting in a non-linear model that follows a series of points and fits the data. When the model assumptions are not satisfied, the statistical method being used may not be appropriate. Therefore, caution must be exercised in assuming the regression model to be correct without first evaluating the residual plots for linearity and testing model assumptions. This is especially important in cases where there are many independent variables relative to the number of observations available for regression model development. If the number of terms approaches the number of observations, the adjusted  $R^2$  will be artificially inflated, making a poor model appear attractive.

## CHAPTER 3

### EQUIPMENT SET-UP AND TESTING

#### 3.1 EQUIPMENT SET-UP

##### 3.1.1 METAL BELLOWS SEAL

Four test sets of various materials, consisting of nickel-based alloys and stainless steels, were evaluated. Test pieces (Figure 3.1) consisted of a 35 convolution bellows core and two end adapters. The end adapters were machined from 316L stainless steel bar stock and designed with flats for placement of three piezoelectric transducers in a triangular arrangement. One adapter was designed with a single flat and end tap while the other was designed with two flats 180° apart and a through tap. Welded to the bellows core by TIG welding, the adapters were located such that the flat planes were parallel.

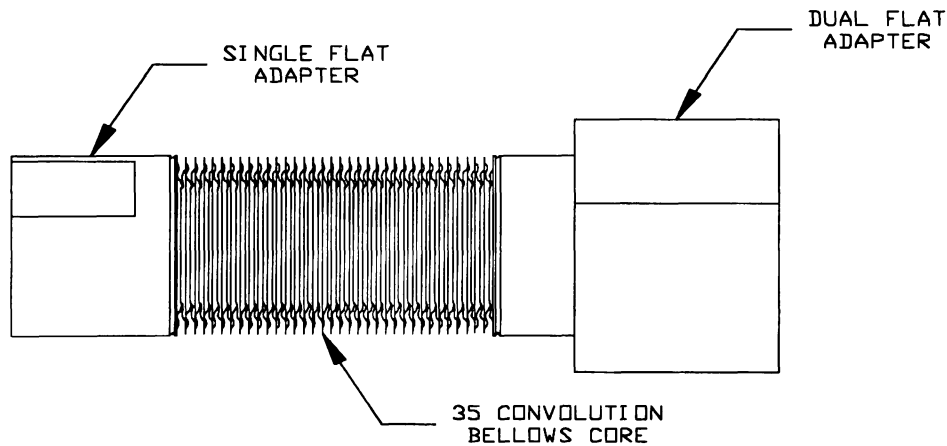


Figure 3.1. Typical metal bellows test specimen.

##### 3.1.2 FINAL ASSEMBLY

The welded assembly was incorporated into a final assembly before installation onto the test bed. It was required to attach a secondary adapter as an interface between the dual flat adapter of the test seal and the load cell. This secondary adapter was designed with grooves for placement of o-rings to seal mating surfaces. The completed final assembly was then installed on the testbed by threading the single flat adapter to the shaft and bolting the

load cell to the support bracket by use of socket-head cap screws. A pressure line was then attached to the load cell for connection to the testbed prior to pressurization of the system.

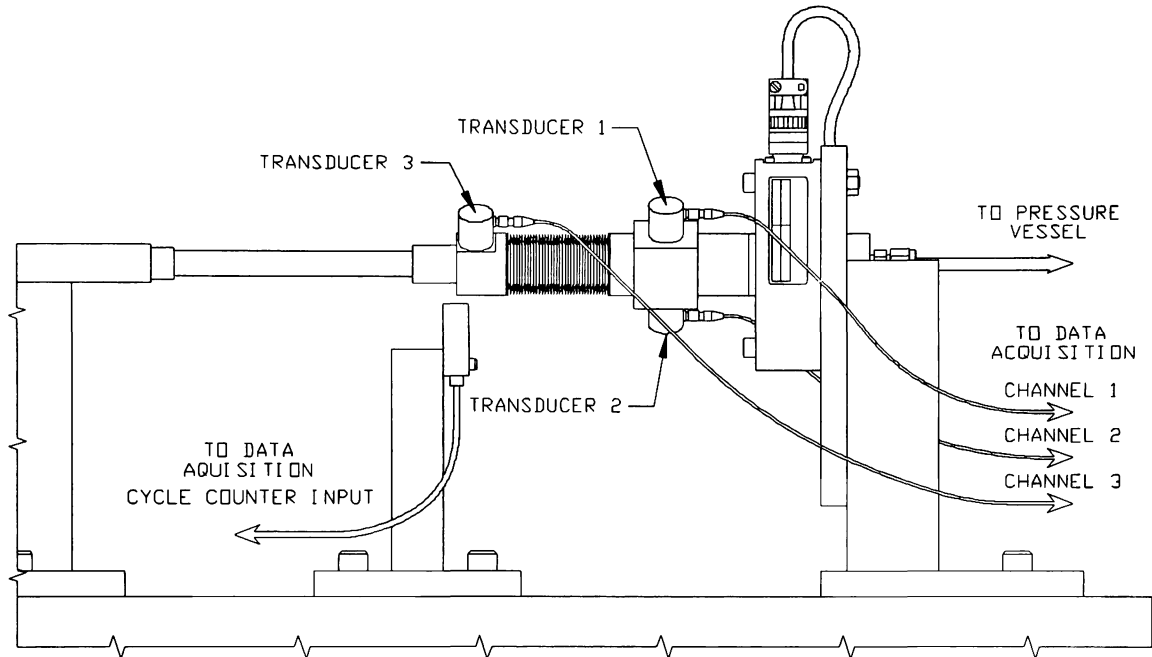


Figure 3.2. Final assembly set-up

### 3.1.3 AE TRANSDUCERS AND PREAMPLIFIERS

Signal waveforms and AE parameter data were collected and filtered by implementing three piezoelectric transducers, with a 150 kHz resonance, and preamplifiers with a 100-300 kHz bandpass filter and 40 dB gain. The transducers were attached to the machined flats of the adapters by use of a thin silicon film which acted as a couplant and adhesive. The transducers' relational positions were calculated to be 21 inches in the horizontal and 1.5 inches in the vertical directions. Flats placement allowed for the transducers to be configured in a triangular arrangement. This arrangement was selected to determine how stress waves propagate through a bellow's complex geometry. If attenuation through the material was minimal, data would be detected by all three sensors. Existing data sets contain the required information for analyzing and determining the regions of highest activity.

### 3.1.4 PRESSURIZATION

Once a metal-bellows test sample was installed on the testbed, the pressure hose was connected to the primary pressure port. A vacuum pump hose was then connected to the secondary port and the pump activated. Evacuation of a pressure vessel beneath the testbed was initiated until a 25 inches Hg pressure reading was noted on the attached pressure gauge. By evacuating the I.D. of the test samples, a stressing condition similar to that of O.D. pressurization could be achieved. In normal operating conditions, the bellows used herein experiences O.D. pressure.

In addition, the system consisted of a pressure sensor that served as a relay to the system power. Incorporated in the sensor was a control setting for maximum allowable system pressure. By setting the pressure sensor at 5 inches of Hg higher than system pressure, an automatic system shutdown would initiate once the sensor detected a pressure increase exceeding the set limit. Figure 3.3 represents the set-up configuration for major components of the testbed.

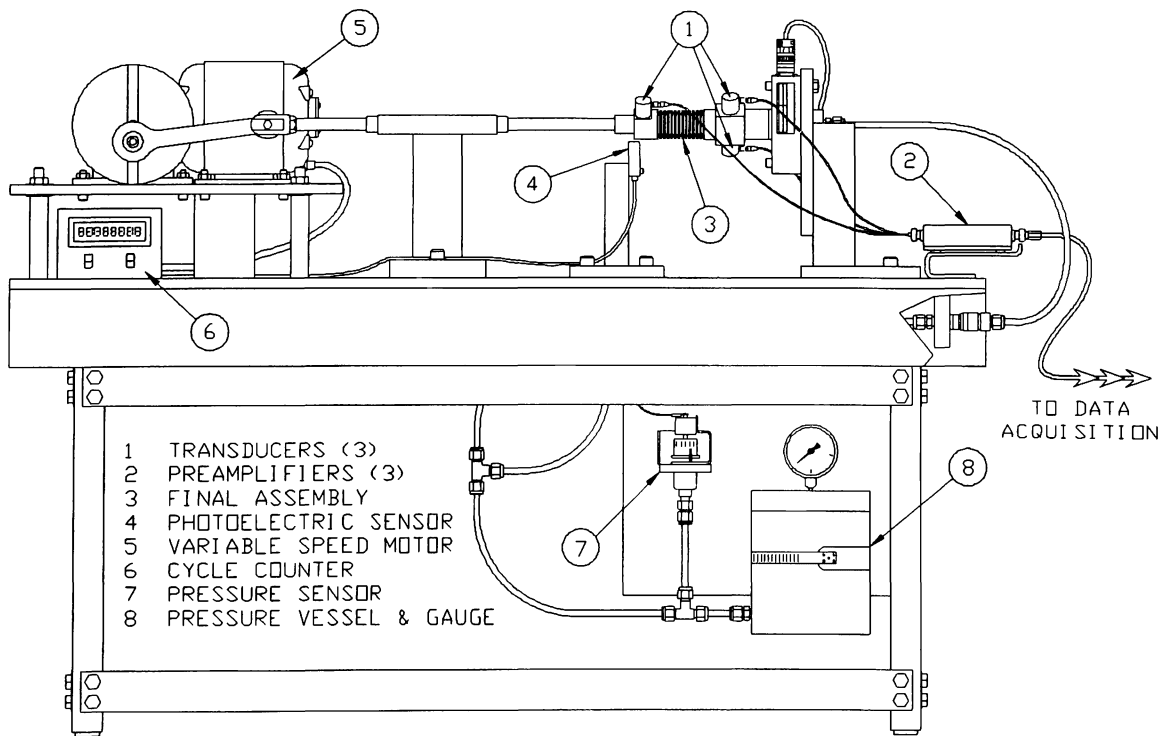


Figure 3.3. Testbed components and set-up configuration.

### **3.1.5 DATA ACQUISITION**

The three transducers, connected to their corresponding preamplifiers, were connected to Channels 1 through 3 on the MISTRAS 2001 data acquisition system card. AE data acquisition settings were as follows: Preamp Gain = 40 dB, Gain = 20 dB, Threshold = 50 dB, PDT = 400  $\mu$ s, HDT = 600  $\mu$ s, HLT = 800  $\mu$ s. Once the test was started, the data acquisition system recorded digitized waveforms and extracted the AE parameters for amplitude, counts, counts-to-peak, duration, energy, and risetime as received on each of the three channels. Standard information of time, date, and channel were also recorded as data were received.

### **3.2 TESTING PROCEDURE**

Changes were incorporated into the test variables to initiate excess stressing within the welds and thereby promote early fatigue failure. These changes consisted of the applied internal vacuum of 25 inches of Hg and an increase of 0.150 inch applied to the extension portion of the bellows stroke length. An AE source simulation technique, the pencil lead break, was performed to check the output of each transducer before test start-up.

Data acquisition and cycling of the test seal were initiated simultaneously. The seal was subjected to a continuous cyclic tension/compression mode. At the time of failure an internal pressure release triggered the system, and shut-down was initiated when the internal vacuum pressure reached 20 inches of Hg. This allowed the leakage signal to be detected, prevented final bellows separation from coloring recorded AE data, and stopped the system at the actual cycle count when material failure occurred.

After failure and system shut-down, the set-up was disassembled and the test specimen inspected for leakage. The failure site was determined by pressurization of the I.D. and applying "snoop" (a soapy solution) to check for bubble formations. The failed section was marked and machined from the bellows core. The section was then mounted and a visual examination of the specimen made to determine if failure occurred within the welded region or within the parent material.



### **3.3 DATA PROCESSING**

Once data were collected by the MISTRAS system, they were visually analyzed for trends in the AE parameters and prepared for use in the neural network analysis. It was necessary, however, to first convert the MISTRAS data files to ASCII format. Once converted, the files could be brought into a spreadsheet program (Excel 7.0 for Windows 95) where all AE parameter data could easily be analyzed. Once an evaluation was made on the data, those data believed to be required for neural network analysis were removed from each test's data set and incorporated into a text file. Text within these files were developed into distributions for the AE parameters evaluated. These distributions were then input for training and testing a back-propagation neural network for prediction of cycle life. A software package produced by NeuralWare, Inc., called NeuralWare Professional II/Plus™, provided the ability to produce neural networks in a graphical environment.

A statistical analysis was then performed on all data sets to determine if a method of regression could accurately predict cycle life. Data sets, consisting of the first 250 hits of each test, were manipulated into a cumulative data table. AE parameters of amplitude, counts-to-peak, duration, energy, and risetime were summed for input into STATGRAPHICS Plus 3.3, a software package that could quickly evaluate and represent the data through statistical analyses, graphing functions, and model development.

## **CHAPTER 4**

### **NEURAL NETWORKS**

#### **4.1 BACK-PROPAGATION NETWORK**

The back-propagation neural network used trains towards a relationship between a set of input vectors and an output vector by attempting to minimize the difference ( $\delta$ ) between the predicted and actual output vectors. Using a gradient descent approach the network is able to learn the correct output vector and its relationship to a series of input vectors. The learning process consists of two phases. First the input vectors are passed through the network to generate a predicted output vector. An error is then computed for each input vector based upon the desired output vector. This error is then back-propagated through the network, upgrading the weights so as to reduce the overall network error. Stopping conditions for back-propagation neural network training are typically set such that the weight changes have reached some minimal value or the average error across a series of input vectors is below some desired level. Models incorporating hyperbolic tangent transfer functions, the activation function used herein, generally aid in generalizing learning characteristics, can positively affect results by accelerating learning for some models, and improve on prediction accuracy.

#### **4.2 BACK-PROPAGATION ARCHITECTURE**

The back-propagation neural network architecture consisted of an input layer, two hidden layers, a fully connected bias, and an output layer (Figure 4.1). The input vector was comprised of a single variable defining material type (0.25 for Inconel 718 and 0.50 for 350 stainless steel) and 51 variables defining the number of hits occurring for each amplitude from 50-100 dB. The output vector consisted of one variable defined as the actual cycle life.

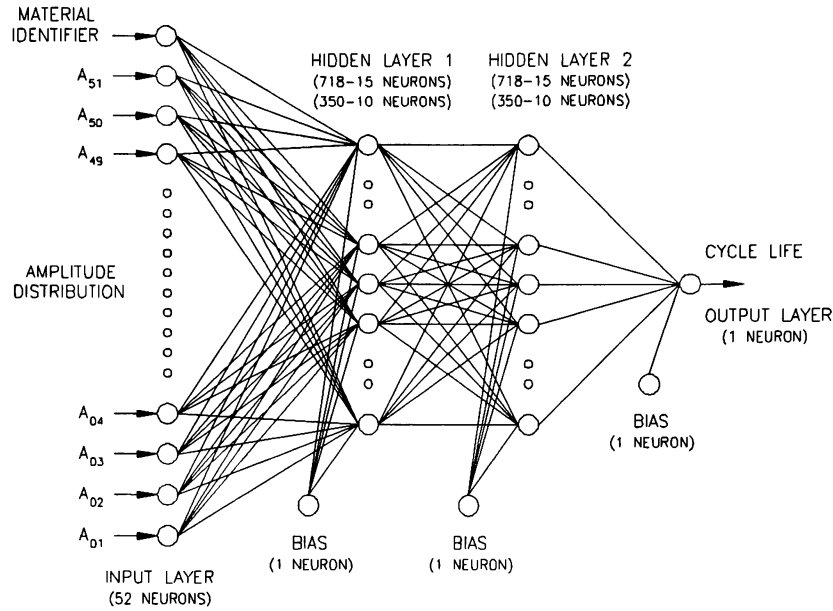


Figure 4.1. Back-propagation neural network used for predicting cycle life.

The number of neurons in the hidden layers have an effect on prediction accuracy. Therefore, an optimization process is generally required to design a network capable of accurate predictions, in this case within  $\pm 5$  percent of the actual cycle life. After optimizing the networks, it was required to modify the number of hidden layer neurons for each material. Inconel 718 was optimized with 15 neurons per hidden layer while the 350 stainless steel required 10 neurons. The number of neurons applied within the hidden layers have an effect on how well the network will fit the training data. If the number of neurons are excessive, the network will fit training data well but will have problems when predicting on the test data. If too few neurons are used, the network will have problems fitting both the training and the test data. A good fit is generally obtained when the errors in fitting the test set are of the same order of magnitude as those from the training set. Due to the low noise levels in the test data, the training error was required to converge near zero to accurately predict on the test data. Once test data resulted in errors below the required 5 percent, the network was considered to be properly trained.

A network is considered “trained” once the weights are adjusted to obtain the required output(s). The purpose of the training is to reach some optimal solution that offers a reasonable prediction within some desired tolerance. Once this requirement is met, the

network can be used as a predictive tool to test on inputs containing patterns recognized and recorded from the training data sets.

### 4.3 BACK-PROPAGATION ALGORITHM

The supervised learning approach is the most commonly used method for training a back-propagation neural network. This approach requires historical data with examples of both inputs and outputs to train the network. It is used to build prediction, classification, and time series models. It is referred to as supervised learning because during training the network can compare the prediction results to the actual results and adjust the model accordingly. The back-propagation algorithm is as follows [Walker et. al. , 1996]:

#### Stage 1 : Forward propagation of input vector

Step 1 : Initialize weights to small random values. Values are generally set between 0 and 1 or -1 and 1 depending on the activation function employed.

Step 2 : When stopping condition is false:

Step 3 : Compute input sum and apply activation function for each middle neuron:

$$y_j = f(W_{ij} * x_i)$$

Step 4 : Compute input sum and apply activation function for each output neuron:

$$z_k = f(V_{jk} * y_j)$$

#### Stage 2 : Back-propagation of error

Step 5 : Compute error:  $\delta_k = (t_k - z_k) * f'(W_{jk} * y_j)$

Step 6 : Compute delta weights:  $\Delta V_{jk} = LC * \delta_k * y_j + \{\text{Momentum} * \Delta V_{jk}(\text{old})\}$

Step 7 : Compute error contribution for each middle layer neuron:

$$\delta_j = \delta_k * W_{jk} * f'(W_{ij} * x_i)$$

Step 8 : Compute delta weights:  $\Delta W_{ij} = LC * \delta_j * x_i + \{\text{Momentum} * \Delta W_{ij}(\text{old})\}$

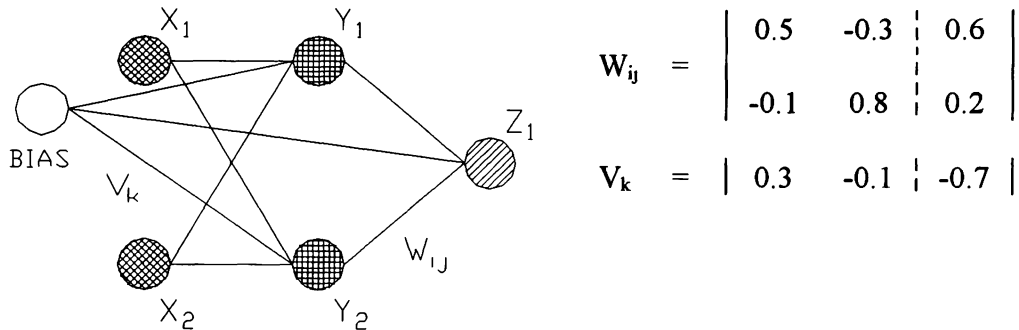
Step 9 : Update weights:  $Q_{rs}(\text{new}) = Q_{rs}(\text{old}) + \Delta Q_{rs}$

Step 10 : Test for stopping condition

Typically, stopping conditions for a back-propagation neural network are when the weight changes or the average error across a series of input vectors have reached some defined minimum.

#### 4.4 BACK-PROPAGATION EXAMPLE

Consider a back-propagation neural network in its most basic form with 2 inputs, a hidden layer consisting of 2 neurons, and a single output as shown below. In this example we wish to find the new weights when the network is presented with an input vector  $x_i = [ 0.0, 1.0 ]$  and a target vector  $Z_1 = 1.0$  using a learning coefficient of 0.05 and a hyperbolic tangent activation function. The weights are randomly initialized as:



Compute the hidden layer output using the relationship  $y_j = W_{ij} * x_i$  :

$$y_1 = (W_{11} * x_1) + (W_{21} * x_2) + W_{1B} = (0.5 * 0.0) + (-0.1 * 1.0) + 0.6 = 0.5$$

$$y_2 = (W_{12} * x_1) + (W_{22} * x_2) + W_{2B} = (-0.1 * 0.0) + (0.8 * 1.0) + 0.2 = 1.0$$

$$Y_{1(OUT)} = f(y_1) = (e^{y_1} - e^{-y_1}) / (e^{y_1} + e^{-y_1}) = 0.462$$

$$Y_{2(OUT)} = f(y_2) = (e^{y_2} - e^{-y_2}) / (e^{y_2} + e^{-y_2}) = 0.761$$

Compute the network output :

$$z_1 = (V_{11} * Y_1) + (V_{12} * Y_2) + V_{1B}$$

$$= (0.3 * 0.462) + (-0.1 * 0.761) - 0.7 = -0.637$$

$$Z_{1(OUT)} = f(z_1) = (e^{z_1} - e^{-z_1}) / (e^{z_1} + e^{-z_1}) = -0.563$$

Compute the network error :

$$\delta_k = \delta_{z_1} = (T_k - Z_k) * f'(Z_1)$$

$$= (Z_1 - Z_{1(OUT)}) * [1 + ( [e^{z_1(OUT)} - e^{-z_1(OUT)}] / [e^{z_1(OUT)} + e^{-z_1(OUT)}] )]$$

$$* [1 - ( [e^{z_1(OUT)} - e^{-z_1(OUT)}] / [e^{z_1(OUT)} + e^{-z_1(OUT)}] )]$$

$$= (1.0 + 0.563) * (1 - 0.510) * (1 + 0.510)$$

$$= 1.156$$

Update middle to output layer weights using  $\Delta V_{jk} = LC * \delta_k * Y_j$  :

$$\Delta V_{11} = LC * \delta_{Z1} * Y_{1(OUT)} = 0.05 * 1.156 * 0.462 = 0.026$$

$$\Delta V_{12} = LC * \delta_{Z1} * Y_{2(OUT)} = 0.05 * 1.156 * 0.761 = 0.044$$

$$\Delta V_{1B} = LC * \delta_{Z1} * Bias = 0.05 * 1.156 * 1.0 = 0.057$$

$$V_{k(NEW)} = \begin{vmatrix} 0.326 & -0.055 & -0.642 \end{vmatrix}$$

Second stage : Compute the middle layer error as  $\delta_j = \delta_k * V_{jk} * f'(Y_j)$  :

$$\begin{aligned} \delta_{Y1(OUT)} &= \delta_{Z1} * V_{11} * f'(Y_{1(OUT)}) \\ &= \delta_{Z1} * V_{11} * [1 + ((e^{Y1(OUT)} - e^{-Y1(OUT)}) / [e^{Y1(OUT)} + e^{-Y1(OUT)}])] \\ &\quad * [1 - ((e^{Y1(OUT)} - e^{-Y1(OUT)}) / [e^{Y1(OUT)} + e^{-Y1(OUT)}])] \\ &= 1.156 * 0.3 * (1 + 0.431) * (1 - 0.431) \\ &= 0.282 \end{aligned}$$

$$\begin{aligned} \delta_{Y2(OUT)} &= \delta_{Z1} * V_{12} * f'(Y_{2(OUT)}) \\ &= 1.156 * -0.1 * (1 + 0.642) * (1 - 0.642) \\ &= -0.067 \end{aligned}$$

Update input to middle layers using  $\Delta W_{ij} = LC * \delta_i * x_j$  :

$$\Delta W_{11} = LC * \delta_{Y1(OUT)} * x_1 = 0.05 * 0.282 * 0.0 = 0.0$$

$$\Delta W_{12} = LC * \delta_{Y1(OUT)} * x_2 = 0.05 * 0.282 * 1.0 = 0.014$$

$$\Delta W_{21} = LC * \delta_{Y2(OUT)} * x_1 = 0.05 * -0.067 * 0.0 = 0.0$$

$$\Delta W_{22} = LC * \delta_{Y2(OUT)} * x_2 = 0.05 * -0.067 * 1.0 = -0.003$$

$$\Delta W_{1B} = LC * \delta_{Y1(OUT)} * Bias = 0.05 * 0.282 * 1.0 = 0.014$$

$$\Delta W_{2B} = LC * \delta_{Y2(OUT)} * Bias = 0.05 * -0.067 * 1.0 = -0.003$$

$$W_{ij(NEW)} = \begin{vmatrix} 0.5 & -0.285 & 0.614 \\ -0.1 & 0.796 & 0.196 \end{vmatrix}$$

Typically, many cycles are required for training a back-propagation neural network. The number of cycles required for training is influenced by the choice of initial random weights. Generally, weights are updated after each training set or number of training sets (batch updating) are presented. By specifying a convergence criterion, or root mean square (RMS) error value, the network will continue to train until a comparison between the predicted value and actual value has meet the specified error level.

## CHAPTER 5

### ANALYSIS AND RESULTS

#### 5.1 AE DATA ANALYSIS

Four sets of metal bellows samples (stainless steels and nickel alloys) were fatigue tested with data taken using acoustic emission (AE) transducers. AE parameter data sets were recorded and analyzed for separation of crack initiation, crack propagation, and turbulent eddies from bellows leakage. Amplitude, duration, and time parameters were determinants for final separation of the various failure mode regions. All failure modes were noted to lie within an amplitude range between 50 and 100 dB, which is typical for ductile metals; however, this variable alone was insufficient for failure mechanism separation. Analyzing the duration versus amplitude plots resulted in surprisingly well separated regions. Plastic deformations associated with fatigue crack initiation were found to have low amplitudes and low durations. Crack propagation had initially low amplitudes and moderate durations progressing toward high amplitudes and long durations. At failure, eddy turbulence had a progression from low to high amplitude with peak durations that remained constant.

Correlations in data and identification of fatigue modes can many times be made by analyzing AE data (amplitude, duration, energy, etc.) for trends in activity. Unfortunately, an analysis of recorded data was found to be inconclusive since no specific trends could be visually identified in the test data. It was concluded that neural networks would need to be implemented to identify any hidden trends which could be correlated to cycle life.

Graphical plots of the AE signal's duration versus amplitude data show typical fatigue crack growth behavior, where Region I represents crack initiation (Figure 5.1); Region II, where stable crack propagation occurs (Figure 5.2); and Region III, where rapid unstable crack growth and failure of the sample takes place (Figure 5.3) [Smith, 1993]. Figure 5.4 represents the final duration versus amplitude plot after vacuum evacuation.

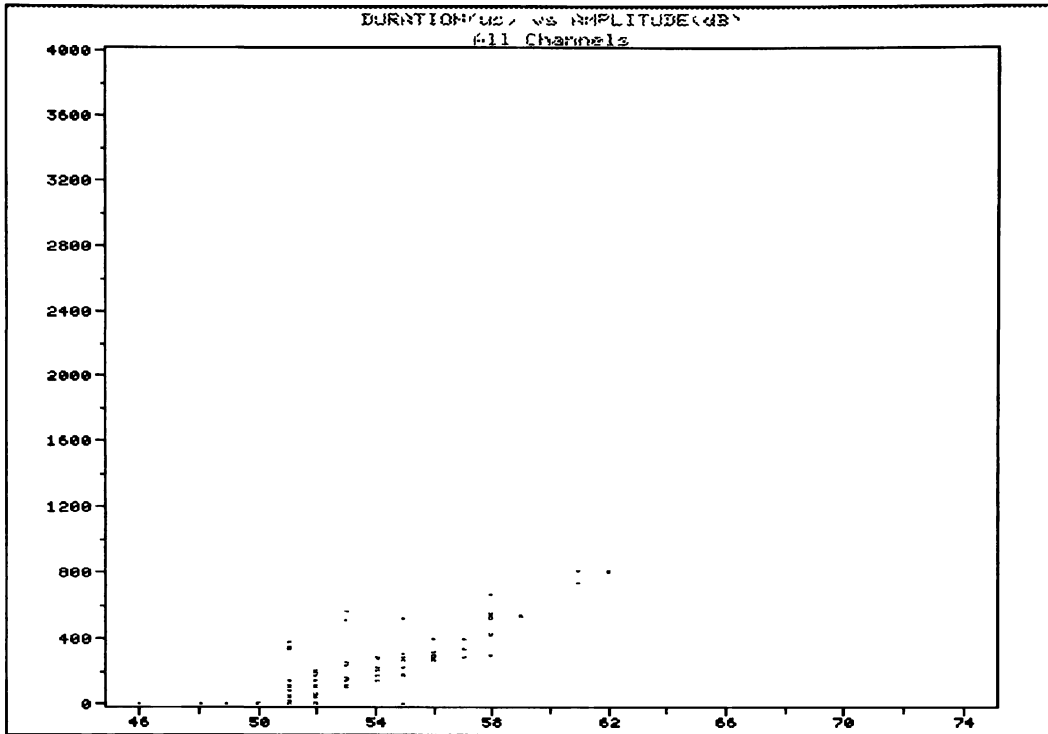


Figure 5.1. Duration versus amplitude plot with crack initiations, Region I events.

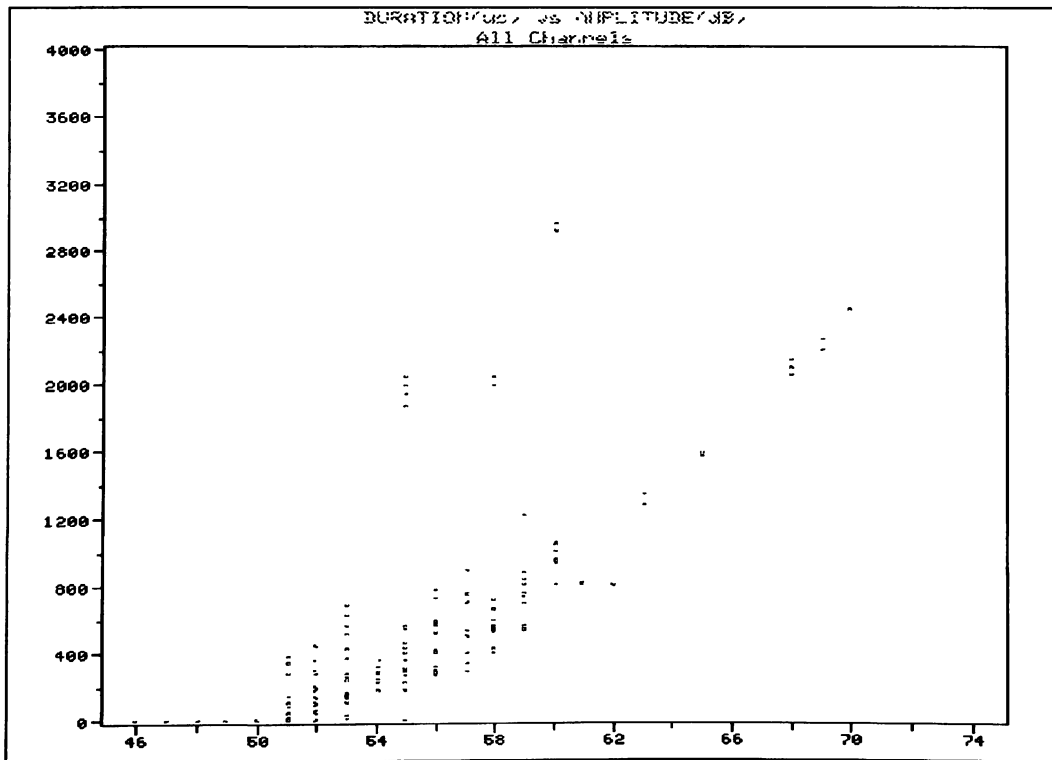


Figure 5.2. Duration versus amplitude plot with stable crack propagations, Region II events.



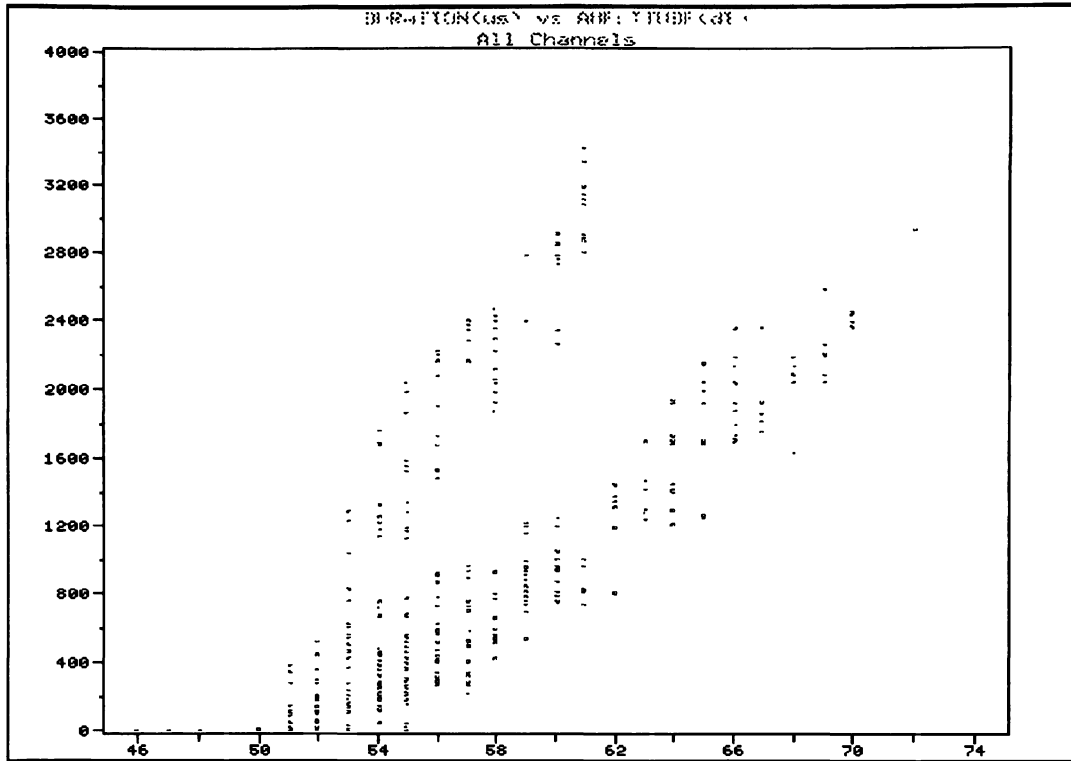


Figure 5.3. Duration versus amplitude plot with rapid crack growth, Region III events.

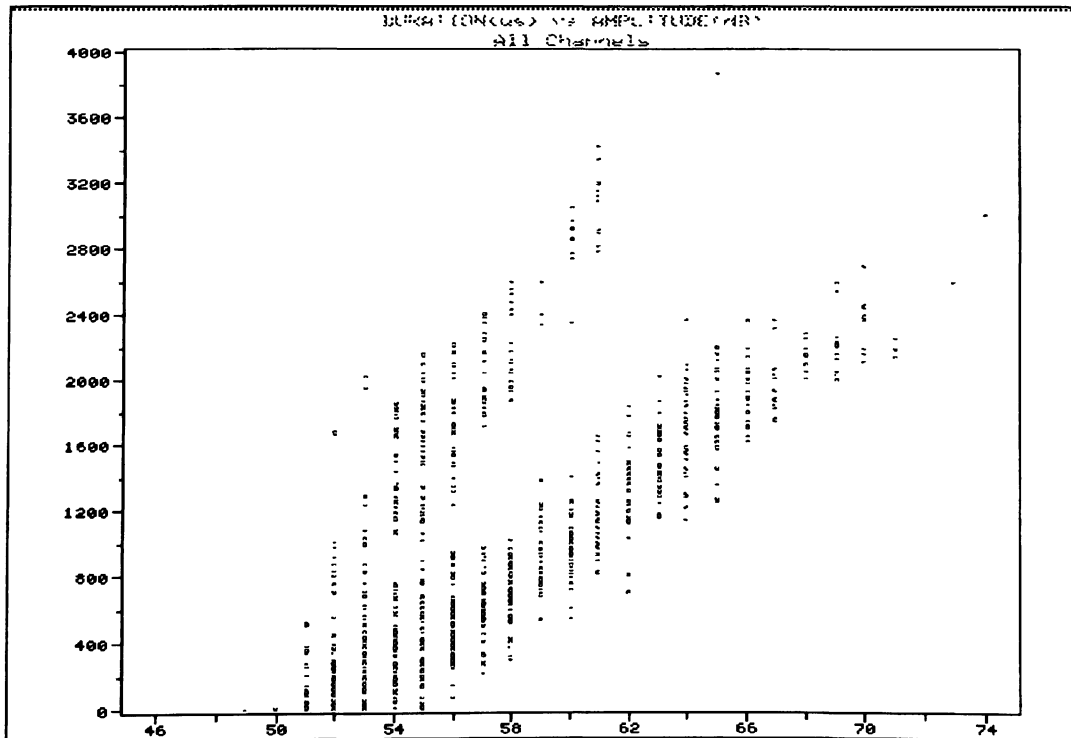


Figure 5.4. Duration versus amplitude plot with vacuum evacuation.

At any one duration, the failure mode tended to have a scattering of approximately 10 dB with the total amplitude ranging from 50 to 80 dB. Outlying hits were occasionally detected between 80 to 100 dB. AE parameters remained constant for crack initiations, Region I events, which consisted of generally short durations ( $< 1000 \mu\text{s}$ ) and short amplitudes (50-60 dB). An increase in hits and durations was evident as events transitioned into crack propagation or Region II events. Crack propagation had initially low durations ( $\approx 1000 \mu\text{s}$ ) that transitioned to moderate durations ( $\approx 3000\text{-}7000 \mu\text{s}$ ). Amplitudes were found to take one of two directions when transitioning through the crack propagation stage. Amplitudes showed moderate change, remaining short (50-60 dB) or had an increase over a longer range (60-75 dB). As rapid crack growth, Region III events, occurred, high amplitudes ( $> 60 \text{ dB}$ ) and long durations ( $> 3000 \mu\text{s}$ ) resulted. At failure, eddy turbulence had a progression from low to high amplitudes (60-80 dB) with low durations ( $\approx 2000\text{-}3000 \mu\text{s}$ ) or durations that progressed to peak values of the test (some tests resulted in durations as high as  $35,000 \mu\text{s}$ ). The magnitude of duration is likely influenced by crack geometry and leakage rate.

In many instances, incoming hits were noted to occur as single channel hits. Signal propagation through the bellows cores consisted of numerous directional changes as a result of bellows geometry. As a result, high attenuation levels were experienced by the hit energy signal and complete propagation was received only by the transducer nearest the source of activity. Thus, source location from the AE data was not possible, in that location can only occur if two or more transducers are able to receive the same AE event.

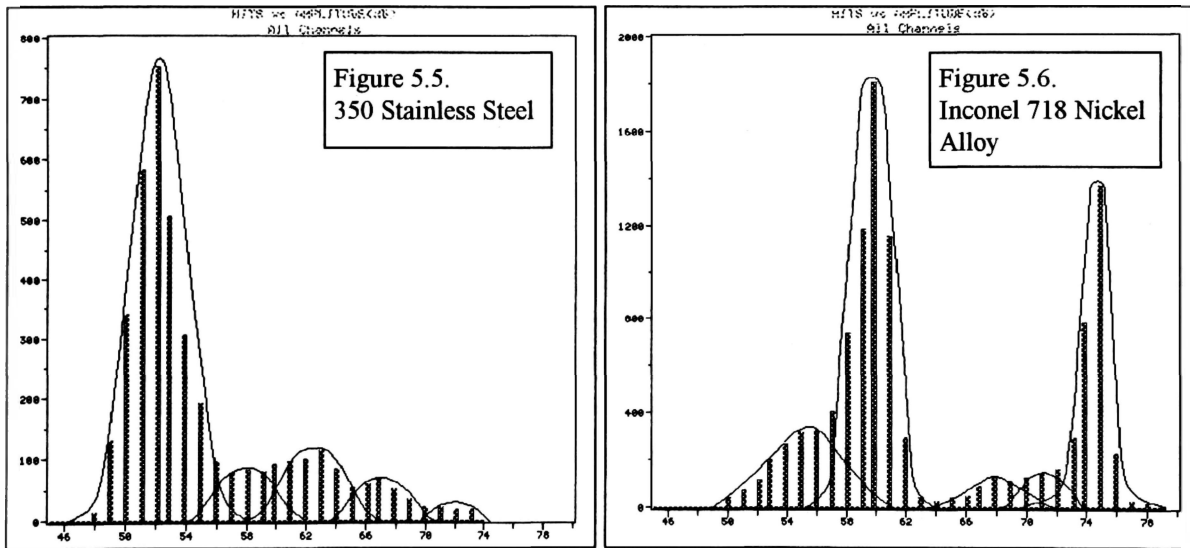
## 5.2 AMPLITUDE DISTRIBUTIONS

The acoustic emission amplitude parameter,  $A$  [dB], is a logarithmic representation of the peak signal voltage,  $V$  [V], of the AE waveform:

$$A = 20 \log ( V / V_i ) \quad (12)$$

For this application,  $V_i = 1 \mu\text{V}$  at the sensor output and is chosen as the 0 dB reference because it is the lowest detectable voltage, just slightly above the noise level of the system electronics [Mitchell, 1984].

Acoustic emission amplitude distributions (hits/events versus amplitude histograms) have been shown to contain information which allows for the identification of failure mechanisms in materials [Pollock, 1981]. The identification comes in the form of “humps” in the amplitude distribution, each of which represents a failure mechanism. For metals, these failure mechanisms include plastic deformation and cracking. As a result of the testing procedure, a third mechanism was observed herein: leakage from release of the internal vacuum as a result of material breakthrough. Figures 5.5 and 5.6 represent test specimens that define the characteristic humps for the 350 stainless steel and Inconel 718 nickel alloy. There appear to be five primary humps for each material with moderate overlap between them.



Figures 5.5 and 5.6. Cumulative hits versus amplitude histogram plots with defined failure mechanism “humps”

The extent of overlap between these regions is a function of the attenuation experienced. Factors such as material properties or geometry are also major factors in the extent of attenuation. In the design of metal bellows, geometry is multidirectional, and as a result, reflective waves are frequent, resulting in attenuation of the output signals. This was proven by the high number of single sensor hits noted within the reviewed results. Fortunately, the amplitude distributions had enough separation in each failure region to allow

for a moderately accurate prediction. Secondly, the data was not considered to be excessively noisy; therefore, a classification of noise from “good” data was not required.

In Figures 5.5 and 5.6 it can be seen that the various failure mechanism humps are comprised of normally distributed AE amplitude bands. These normalized distributions are the result of measurements being taken as logarithms, which tend to have such distributions [Tennant-Smith, 1985]. Approximations for 350 stainless steel (Figure 5.5) show two failure mechanism humps from 45-62 dB due to plastic deformation, two failure mechanism humps from 58-71 dB associated with crack initiations and propagations, and one failure mechanism hump from 70-75 dB due to leakage. Approximations for Inconel 718 nickel alloy (Figure 5.6) show two failure mechanism humps from 49-64 dB due to plastic deformations, two failure mechanism humps from 63-79 dB associated with crack initiations and propagations, and one failure mechanism hump from 70-75 dB due to leakage. Overlap within the amplitude distributions requires the use of neural networks to determine the contribution of each mechanism.

### **5.3 FATIGUE ANALYSIS**

Inspection of failure sites revealed typical ductile failures occurring at the inner diameter (I.D.) welds within the heat affected zone (HAZ). I.D. weld failures were expected due to the alternating stresses placed on the welds by the cyclic loading and applied internal vacuum. Finite element analysis models have supported this observation, showing the highest stresses to be located at the I.D. welds. In extension, maximum stresses focus at the I.D. on the inner and outer walls of the diaphragm (Figure 5.7).

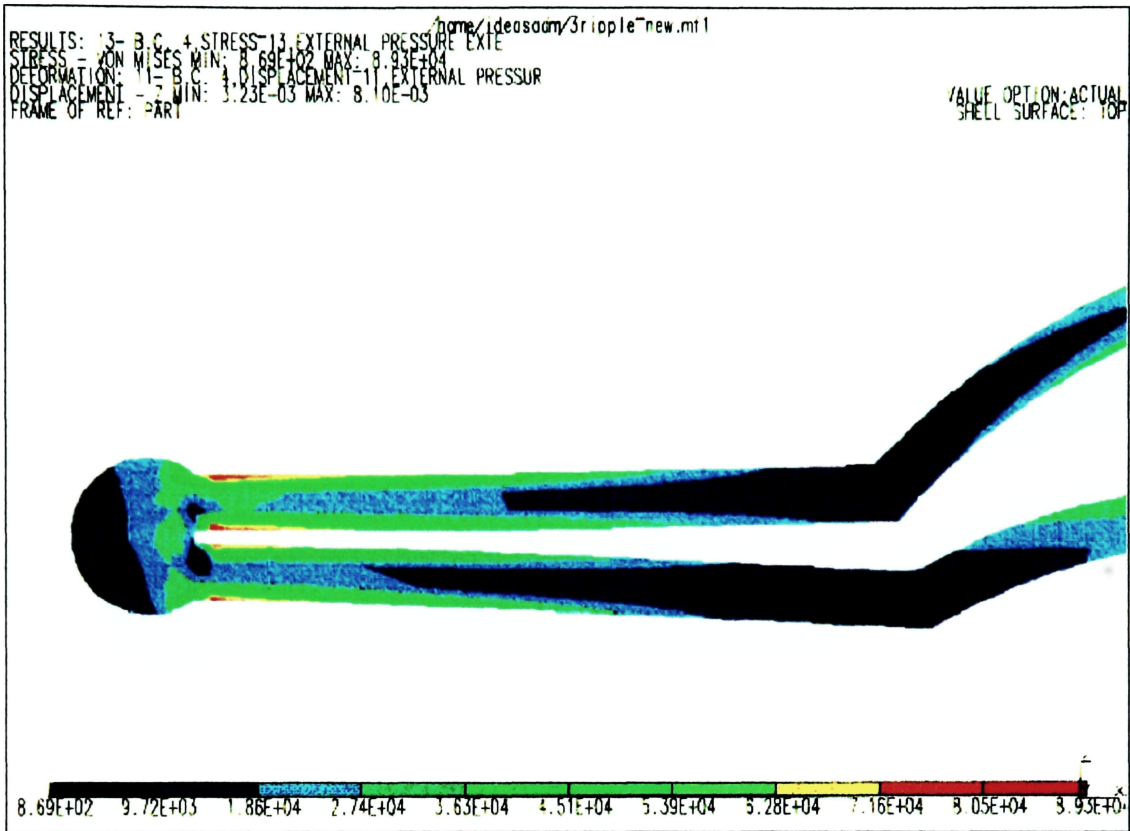


Figure 5.7. Stress distribution at I.D. weld during stroke at maximum extension.

In compression, stresses shift to the flat and first I.D. ripple transition (Figure 5.8). Such cyclic stressing results in the material undergoing a plastic deformation and embrittlement process. A period is observed where no AE activity is evident. Within this period the material undergoes a stage of strain-hardening. The material's dislocation density increases with deformation resulting in a reduction in dislocation movements. This results in an increase in tensile strength and a decrease in ductility of the material. As strain hardening increases within the material, a critical point is achieved where fatigue cracking (a brittle failure mechanism in a normally ductile material) occurs, and high levels of AE activity are evident.

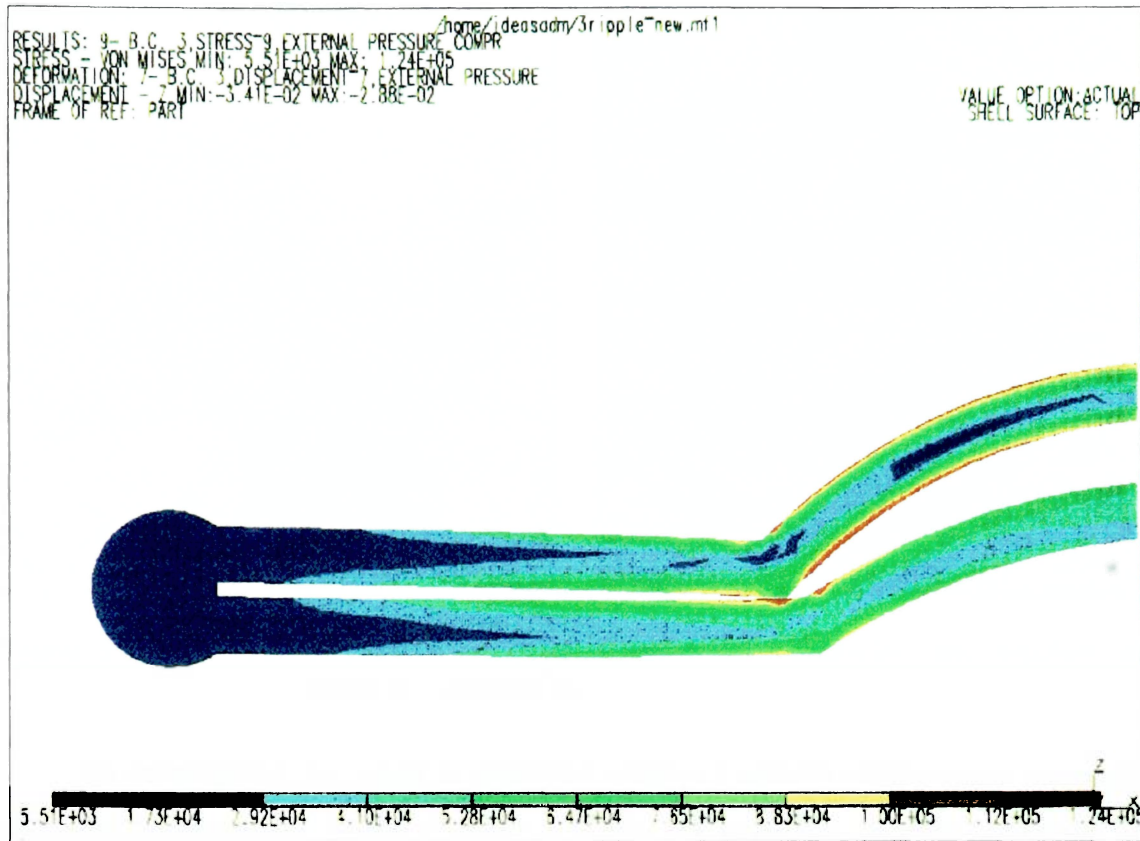
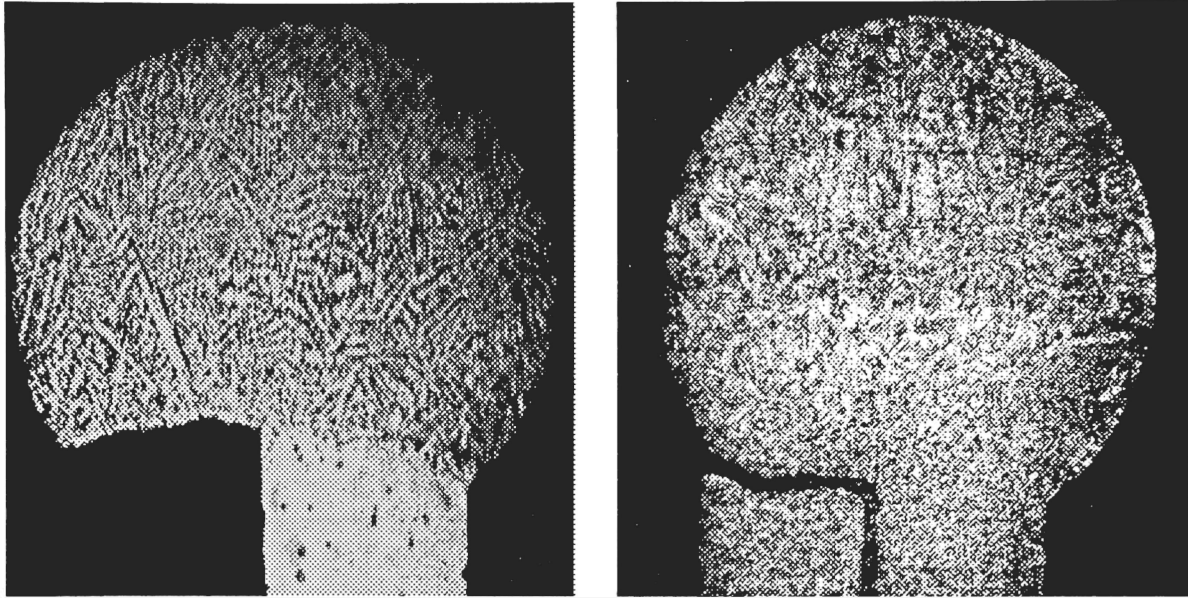


Figure 5.8. Stress distribution at I.D. weld during stroke at maximum compression.

Mounted sections were evaluated at the site of failure. All failures occurred within the heat-affected zone (HAZ), a region that experiences reduced material strength as a result of transitional changes in grain structure due to welding. Weld failures were prevalent at I.D. locations, typical for the applied pressure conditions of these tests. Figures 5.9 and 5.10 represent typical failures for the nickel alloy and stainless steel specimens, respectively.



Figures 5.9 and 5.10. Typical HAZ region failures for nickel-alloy and stainless steel materials, respectively.

An investigation was made to determine whether a bellows experiences a nonuniform loading or displacement within a stroke. It was hypothesized that the existence of a nonuniformity would be consistent with failures occurring at a specific region of the bellows core. Regions of interest were the stationary and moving ends of the bellows. It is generally accepted that a bellows can be evaluated as a spring when analyzing loading conditions. Therefore, a uniformly distributed loading and linear displacement would exist as a compressive or tensile force is applied.

After each test specimen experienced failure, a leak test was performed to determine the failure site. Table 5.1 lists specimen identifications and failure locations, noted from the dual flat adapter, for the four materials tested. Figure 5.11 represents a histogram of failure locations for all materials tested. Failure locations tended to be higher in occurrence on the fixed end with the remainder of occurrences scattered. An excessive loading condition or a nonlinear displacement may exist in this region of highest occurrence. To support such an argument, however, a larger data set would need to be evaluated in order to verify that occurrences have a tendency to localized in this region.

Table 5.1. Failure locations for each test specimen with reference to the dual flat adapter.

TEST IDENTIFICATION	MATERIAL	FAILURE LOCATION
0100	350 stainless steel (NHT)	16th I.D. weld
0200	350 stainless steel (NHT)	2nd I.D. weld
0300	350 stainless steel (NHT)	21st I.D. weld
0400	Inconel 625 nickel alloy	15th I.D. weld
0500	Inconel 718 nickel alloy	2nd I.D. weld
0600	Inconel 718 nickel alloy	2nd I.D. weld
0700	Inconel 718 nickel alloy	3rd I.D. weld
0800	350 stainless steel (HT)	5th I.D. weld
0900	350 stainless steel (HT)	8th I.D. weld
1000	350 stainless steel (HT)	10th I.D. weld
1100	Inconel 625 nickel alloy	16th I.D. weld
1200	Inconel 625 nickel alloy	34th I.D. weld
1300	Inconel 625 nickel alloy	5th I.D. weld
1400	350 stainless steel (HT)	24th I.D. weld
1500	350 stainless steel (HT)	6th I.D. weld
1600	350 stainless steel (HT)	30th I.D. weld
1700	350 stainless steel (HT)	13th I.D. weld
1800	Inconel 718 nickel alloy	10th I.D. weld
1900	Inconel 718 nickel alloy	2nd I.D. weld
2000	Inconel 718 nickel alloy	24th and 33rd I.D. welds
2100	Inconel 718 nickel alloy	2nd I.D. weld
2200	350 stainless steel (HT)	5th I.D. weld
2300	350 stainless steel (HT)	14th and 24th I.D. welds
2400	350 stainless steel (HT)	8th I.D. weld
2500	350 stainless steel (HT)	21st I.D. weld
2600	350 stainless steel (HT)	1st I.D. weld
2700	350 stainless steel (HT)	8th I.D. weld
2800	350 stainless steel (HT)	5th I.D. weld

NHT = non-heat treated      HT = heat treated



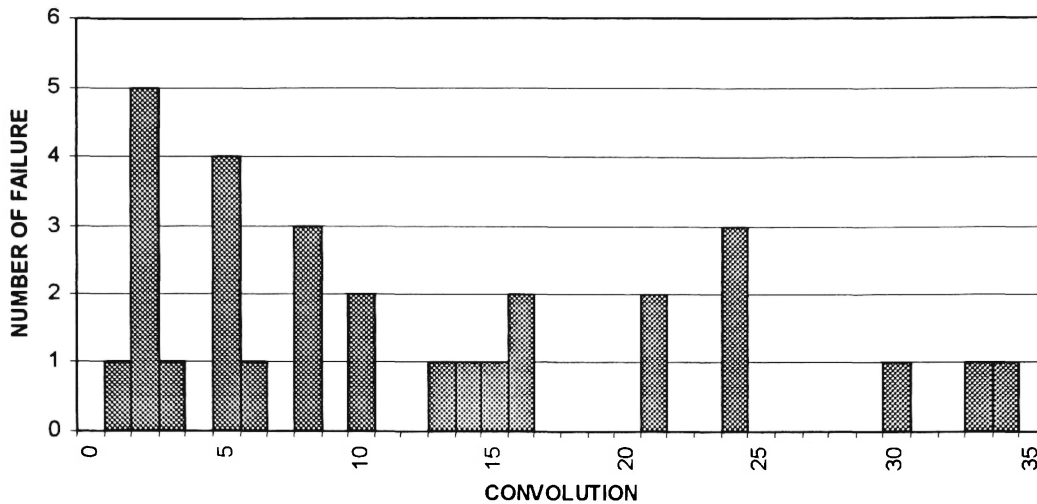


Figure 5.11. Histogram of weld failure locations for all materials tested. Convolution number is with reference to the dual flat adapter.

#### 5.4 NEURAL NETWORK RESULTS

The AE variable of amplitude has proven to be effective for prediction. When formed into an amplitude distribution, a neural network has been successful in identifying trends and predicting burst pressures in composite pressure vessels [Hill, 1992]. From each test conducted herein, amplitude distributions were developed for the first 100, 250, 500, and 1000 hits. Evaluation of each distribution set resulted in the conclusion that the 250 hit distributions were most effective for prediction. All other distribution sets tended to have one or more predictions with a percent error above 15 percent, some as high as 200 percent. It is believed the 100 hit amplitude distributions did not contain sufficient data for the neural network to characterize trends. The 500 and 1000 hit amplitude distributions were believed to result in poor prediction due to the presence of numerous failure mechanisms. Several tests failed with less than 1000 total hits; therefore, these distributions included an increased percentage of amplitude data consisting of crack propagation failure mechanisms.

Final AE parameter data consisted of the amplitude distribution, in 1 dB increments (50-100 dB) for the first 250 hits (Table 5.2), and the final cycle life. Amplitude distributions were used as network inputs while actual cycle lives were supplied as target values for the supervised training phase.

Each material, Inconel 718 nickel alloy and 350 stainless steel, consisted of seven tests that were used to train and test a back-propagation neural network for prediction of bellows cycle life. The network was structured with an input layer consisting of the amplitude distribution data, two hidden layers for mapping failure mechanisms, and an output layer containing the target cycle life. The trained network was then applied to the remaining tests to determine if cycle life could accurately be predicted.

Table 5.2 : Training and testing data for Inconel 718 and 350 stainless steel test specimens.

TEST ID / MATERIAL	CYCLES TO FAILURE	AMPLITUDE DISTRIBUTION DATA (50-100 dB)*
0500 / Inconel 718	91,145	52 27 37 23 23 18 12 9 9 9 7 6 1 3 5 1 1 3 2 1 1 0
0600 / Inconel 718	40,073	44 65 99 33 8 1 0
0700 / Inconel 718	67,660	36 83 113 12 1 1 3 0 1 0
1800 / Inconel 718	51,818	18 12 13 11 13 13 13 16 22 18 5 10 7 15 15 9 7 6 4 3 3 3 6 5 1 0 2 0
1900 / Inconel 718	25,252	8 9 18 18 27 17 5 5 3 7 8 6 5 15 10 17 16 20 20 6 3 3 2 0 1 0 0 0 0 0 0 0 0 1 0
2000 / Inconel 718	11,392	12 20 35 32 32 35 25 9 16 5 10 6 2 1 2 0 0 0 3 1 3 0 1 0
2100 / Inconel 718	27,216	5 9 14 32 34 42 49 27 7 3 15 13 23 4 1 0 0 1 1 0 0 0 0 0 1 0 1 0 0 1 0 0 0 0 0 0 0 0 0 0 0 1 1 0 1 0 0 0 0 0 0 0 0 0 0 0 0 0 0
0800 / 350 S.S.	213,668	40 36 42 18 16 16 6 7 3 5 2 4 3 4 2 4 6 4 2 4 2 0 1 0 3 2 1 1 2 3 1 2 0 0 3 2 0
0900 / 350 S.S.	82,428	49 97 72 8 4 3 1 1 2 0 1 0 1 2 0 0 1 0 0 1 0 0 0 0 0 0 1 1 0 1 0 0 1 0 1 0 0 0 0 0 0 1 0 0 0 0 1 0 0 0 0 0 0 0 0 0 0 0 0 0 0 0 0 0
1000 / 350 S.S.	108,950	30 29 22 15 6 6 5 5 5 6 3 7 1 0 1 1 3 1 0 0 0 0 0 0 1 0 2 2 0 0 1 0 0 2 1 0 0 0 1 0 1 0 0 0 0 0 1 0 0 0 0 0 0 0 0 0 0 0 0 0 0 0 0
1400 / 350 S.S.	265,803	30 23 4 5 4 9 25 51 81 17 1 0
1500 / 350 S.S.	92,718	47 36 57 31 10 5 1 0 5 15 20 8 2 3 1 4 2 0 0 0 0 0 0 0 0 0 0 1 0 0 0 0 0 0 0 0 1 0 0 0 0 0 0 0 1 0 0 0 0 0 0 0 0 0 0 0 0 0 0 0 0 0
1600 / 350 S.S.	511,702	32 11 35 27 23 27 20 20 19 16 12 3 0 1 0 0 1 0 1 0 0 0 1 0 0 0 0 0 0 0 0 0 0 0 0 0 0 1 0
1700 / 350 S.S.	303,948	61 16 21 12 10 20 10 13 10 7 11 11 6 3 3 5 3 4 1 3 3 2 5 3 2 2 0 1 0 1 0 0 0 0 0 0 0 0 1 0

\* Amplitude distributions consist of the first 250 hits occurring within a test. Tests having less than 250 total hits have amplitude distributions consisting of the total number of hits.

Table 5.3 represents the neural network settings used in the training and testing stages. The network required training on four samples for the Inconel 718 and five samples for the 350 stainless steel. Once trained the network was able to predict cycle life with a worst case error

of -4.45 percent and 2.66 percent for the Inconel 718 and 350 stainless steel, respectively. A secondary validation set of samples (Tests 2200 and above) was obtained for the 350 stainless steel and applied to the trained network. Three of the five samples fell within the  $\pm 5$  percent error requirement, but two samples failed with large errors. Table 5.4 represents a summary of the actual and predicted cycle life values for samples tested by the trained networks.

Table 5.3 : Neural network training and testing parameters

PARAMETER	INCONEL 718	350 STAINLESS STEEL
Input Layer Neurons	52	52
Hidden Layer 1 Neurons	15	10
Hidden Layer 2 Neurons	15	10
Output Layer Neurons	1	1
Bias	YES	YES
Learning Coefficient	0.005 / 0.010 / 0.010	0.035 / 0.035 / 0.005
Learning Rule	Normalized-Cumulative-Delta	Normalized-Cumulative-Delta
Transfer Function	Hyperbolic Tangent	Hyperbolic Tangent
Momentum	0.400	0.400
Transition Point	5000	5000
Learning Coefficient Ratio	0.500	0.500
F' Offset	0.100	0.500
Min-Max	YES	YES
Convergence Criterion	0.010	0.020
Epoch Size	4	3 *
Input Range	0.000 to 1.000	0.000 to 1.000
Output Range	-0.800 to 0.800	-0.800 to 0.800
Cycles to Learn	2869	1950

\* Epoch size does not reflect the number of test samples (5 samples) used in network training.

Table 5.4 : Summary of the network testing results

Test ID / Material	Actual Cycle Life	Predicted Cycle Life	Percent Error
0700 / Inconel 718	67,660	64,649	-4.45
1900 / Inconel 718	25,252	24,556	-2.76
2100 / Inconel 718	27,216	27,981	2.81
0800 / 350 Stainless	213,668	219,352	2.66
1000 / 350 Stainless	108,950	107,451	-1.38
2200 / 350 Stainless	53,511	51,402	3.94
2300 / 350 Stainless	33,181	73,728	122.20
2400 / 350 Stainless	48,104	30,420	-36.76
2500 / 350 Stainless	226,774	225,432	0.59
2800 / 350 Stainless	111,673	114,113	-2.19

## 5.5 MULTIPLE LINEAR REGRESSION ANALYSIS

A comparison was made on the results of the neural network and a standard statistical method, multiple linear regression. In the statistical analysis, all materials were initially evaluated to see if a single model could be used for prediction on multiple materials. Before attempting such an analysis, a scatterplot matrix was developed using all variables of interest in the analysis (Figure 5.12).

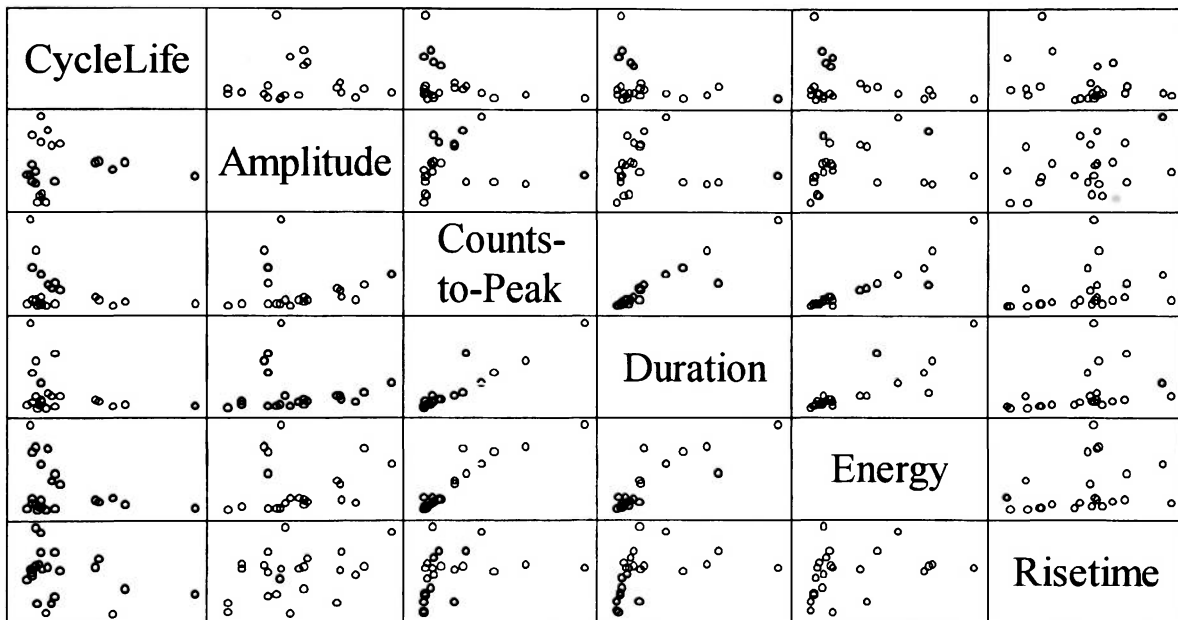


Figure 5.12. Scatterplot matrix for comparison of AE parameters.

A scatterplot matrix aids in identifying paired linear or nonlinear relationships between independent variables. Generally, variables which show linear relationships have a strong correlation with one another. If strong multicollinearity exists between two or more variables, only one is required in the model to reflect the effect of all variables with the linear relation. Generally, a simple linear regression is used with each independent variable and the variable with the greatest prediction ability, or  $R^2$  value, is incorporated into the multiple linear regression model.

Cases do exist, however, that require transforming data through the use of a transfer function (i.e., logarithmic, exponential, reciprocal). Evaluation of the scatterplot matrix identified three variables (counts-to-peak, duration, and energy) that showed strong linear relationships. Unfortunately, the dependent variable of interest, cycle life, showed no such

relationship to these variables. To determine which variable would be incorporated into the multiple linear regression model, a simple linear regression was performed using each of the three variables. Statistical analysis showed the variable of energy to have the best prediction with an  $R^2$  value of 9.206 percent, as opposed to the 8.723 and 8.404 percentages calculated for counts-to-peak and duration, respectively

Multiple linear regression was the method selected to model an equation for prediction. A secondary scatterplot was created with only the variables of interest (cycle life, amplitude, energy, and risetime) incorporated (Figure 5.13).

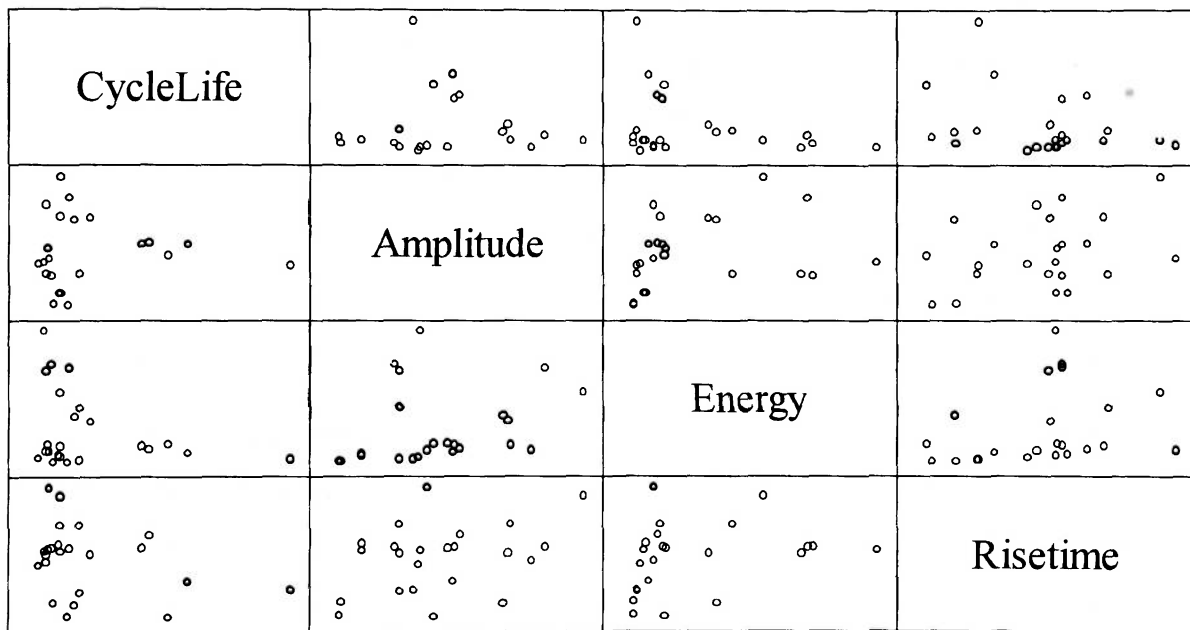


Figure 5.13. Final scatterplot matrix for multiple linear regression analysis

In the second scatterplot, an exponential trend was seen in the cycle life versus amplitude, versus energy, and versus risetime plots. A clustering of data points was noted to occur in the lower left region of each plot. There has been no defined correlation that explains this region separation; however, it has been hypothesized that the unidentified variable may be related to changes in material properties and/or weld geometry. All clustered data within the lower left region are representative of low cycle life and low occurrence of variables. All Inconel 718, one Inconel 625, and two 350 stainless steel samples were noted to exist in the clustering. Therefore, the characteristic of the “missing” variable tends to have an effect on all materials

evaluated. This raises the question: Does variability in material lots or manufacturing processes have an effect on which region a sample clusters into?

An appropriate model, with sufficient predictability, cannot be developed using both the data in the exponential and clustered regions. By looking at the data within the clustered region, a linear relationship would be inappropriate. The fitted line would be horizontal, therefore, for any value of  $x$  the best possible prediction for  $y$  would be to use the resulting average of all  $y$  values. Until a larger data set can be supplied to better develop the trend existing in this region, an accurate model for prediction cannot be developed. As a result, the data set was simplified and a statistical analysis made only on data in the exponential region.

Since the curve tended to be exponential, a natural log transformation was applied to each variable and a regression model performed using the STATGRAPHICS software. The software developed regression models for all possible combinations of the set of variables. In the analysis, three variables (amplitude,  $x_1$ ; energy,  $x_2$ ; and risetime,  $x_3$ ) were evaluated and two incorporated in the final model. From the analysis the model was given as:

$$y = 114095000 - 11807800 \ln x_1 - 9934850 \ln x_2 + 1028750 \ln x_1 \ln x_2 \quad (13)$$

This model resulted in an adjusted  $R^2$  capable of explaining 98.2 percent of the total variation in the  $y$  values. The  $p$ -value was found to be less than 0.01, therefore, there was a statistically significant prediction ability associated with the model. The model was evaluated for significance by reviewing the  $C_p$  statistic. The  $C_p$  statistic can be used to gain insight on the adequacy of a candidate model by comparing to the total number,  $p$ , of  $\beta_i$  parameters in the model. For example, a  $C_p > p$  indicates a model that is biased due to being underfitted (chosen too few model terms) or one with excessive prediction variance from overfitting (has redundancies in the model), while a  $C_p$  approximately equal to  $p$  indicates a reasonable model [Walpole et. al., 1993]. The selected model was found to have a  $C_p$  of 4.6, close to the number of parameters (4) in the model. The Durbin-Watson statistic is a measure used to test a model for autocorrelation between variables. Developed with a scale of 0 through 4, a 0 or 4 represents the highest level of autocorrelation while a value of 2 is desirable and represents the lowest level of autocorrelation. The selected model was found to have a Durbin-Watson statistic of 2.54, therefore, a low level of autocorrelation existed in the model.

Plots were created for the residuals to evaluate if constant variance and normality existed in the distributions. Figure 5.14 represents studentized residuals versus predicted cycle life and Figure 5.15 represents the normal probability plot of the studentized residuals.

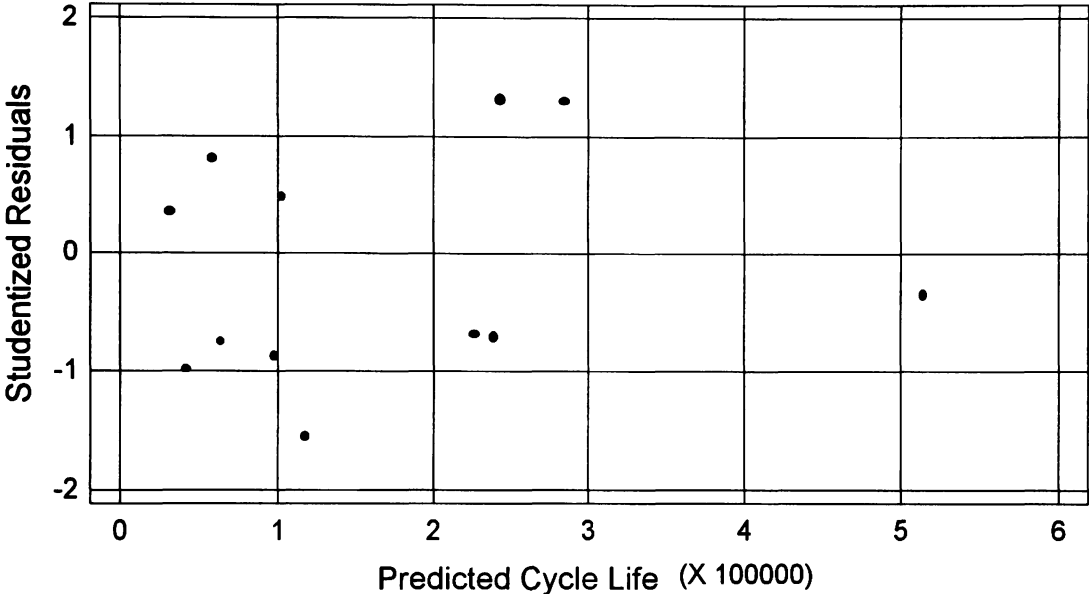


Figure 5.14. Plot of studentized residuals versus predicted cycle life.

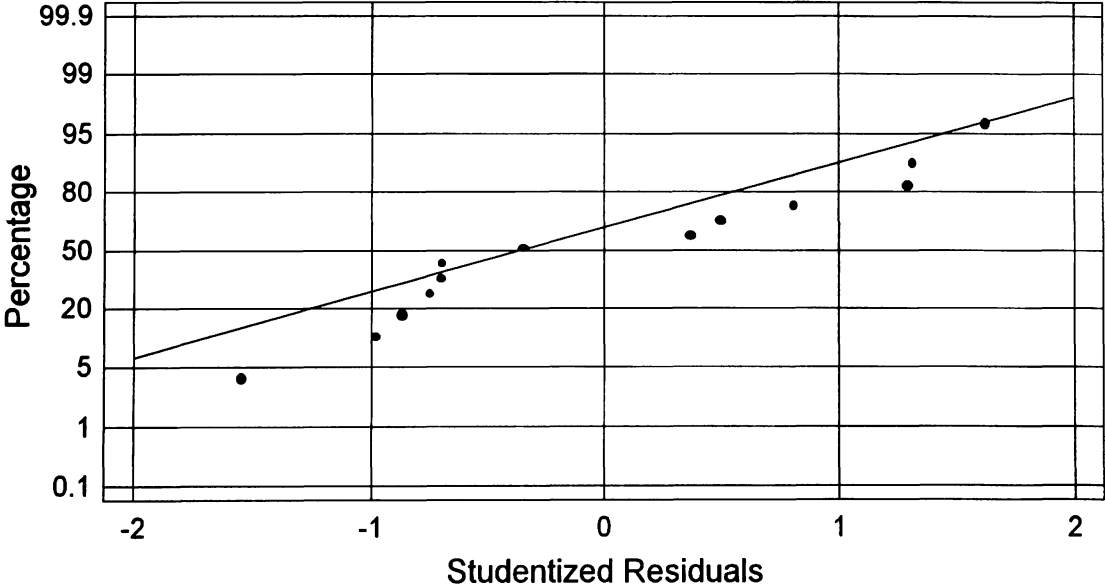


Figure 5.15. Normal probability plot for studentized residuals.

The plot in Figure 5.14 does show random scatter; however, Figure 5.15 shows a scatter focused more to the lower region of the line. It can only be said that there exists constant variance in the studentized residuals distribution, but a larger data set must be evaluated to confirm there is sufficient normality in the studentized residual distribution.

Figure 5.16 represents a plot of the linear prediction model and actual cycle life values. A uniform scattering of data points lie fairly close to the line. Therefore, it looks as though the model has a significant prediction ability.

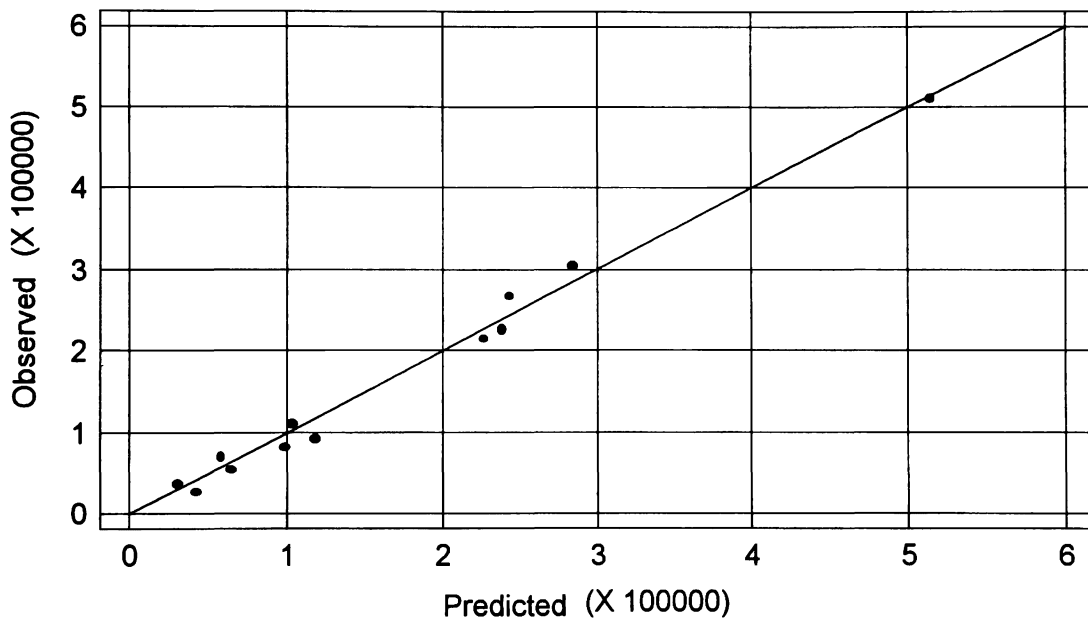


Figure 5.16. Plot of observed cycle life versus predicted cycle life.

To determine whether the model does has significant prediction ability, the following hypothesis test for the  $\beta_i$  coefficients was performed:

$$H_0 : \beta_1 = \beta_2 = \beta_3 = 0$$

$$H_a : \text{at least one } \beta_i \neq 0$$

Examination of the analysis of variance (ANOVA) table developed in Statgraphics revealed a F-ratio of  $F = 217.01$ . Using a F-distribution statistical table for the number of observations  $n = 13$ , the number of variables  $k = 3$ , and the area to the right of the normal distribution of  $\alpha = 0.05$ ; the f-distribution  $[f_{\alpha}(k, n-k-1)]$  was found to be  $f_{0.05}(3, 9) = 3.86$ . This value is much smaller than the calculated F-ratio of 217.01; hence, our statistic falls far outside the interval.



The corresponding p-value was much less than the  $\alpha$  of 0.05. Therefore, we can reject the null hypothesis that there is no significant prediction ability for the model and accept the alternate that at least one of the variables has significant prediction ability.

To determine whether all  $\beta_i$  parameters are necessary, a hypothesis test was conducted for each parameter as follows:

$$H_0 : \beta_i = 0$$

$$H_a : \beta_i \neq 0$$

Since each individual  $\beta_i$  was evaluated, a more liberal  $\alpha$  of 0.10 was used. The p-value for each parameter was much less than 0.10 ( $\beta_1$ ,  $p = 0.0013$ ;  $\beta_2$ ,  $p = 0.0013$ ;  $\beta_3$ ,  $p = 0.0014$ ). Consequently, it can be concluded that each parameter has significant prediction ability and is required in the model.

## CHAPTER 6

### CONCLUSIONS AND RECOMMENDATIONS

#### 6.1 CONCLUSIONS

The application of neural networks and multiple linear regression for predicting cycle life are promising with the results obtained thus far. However, to accurately test the ability of these methods, testing with larger data sets should first be performed. The low error results obtained in these tests are questionable. Studies on neural networks have shown testing with too small a data set can result in accurate predictions on the testing data but poor prediction on secondary sets of validation data. In cases where very small data sets are used, a neural network can train itself to guess near zero error many times and achieve a good rate of prediction [NeuralWare, Inc., 1995]. Although an equation was found to fit the data set evaluated in the statistical analysis, a larger data set should be applied to the equation to confirm the accuracy of the model. With a larger data set, the equation may require modification for a best fit.

Initial testing offered results with predicted cycle lives meeting the accuracy requirement of  $\pm 5$  percent error. However, continued testing within this research project has presented a dilemma. A second set of seven test samples for the 350 stainless steel was run through the trained network. This second set of test samples consisted of two separate runs of the 350 stainless steel material. These tests resulted in several samples failing the requirement of accurately predicting cycle life within  $\pm 5$  percent. This is believed to be due to two factors: (1) new material, geometry, and/or manufacturing variations were present in the new lot of material and product; and (2) the new variations were not tested on and incorporated into the neural network model; therefore, the network could not predict accurately.

### **6.1.1 FAILURE MECHANICS**

- Bellows crack propagation is not constant, but cyclic over time. The material experiences “quiet” periods of no AE activity, followed by shorter periods of high AE activity. A cycle of strain-hardening and material fatigue results. Stainless steel materials see multiple cycles of high to low AE activity, while nickel alloy materials experience a single cycle of strain hardening and an immediate final failure.
- Cycle life is greatly affected by whether a material is heat treated or non-heat treated. Heat treatments increase material strength but compromise cycle life by reducing ductility. Heat treated materials tend to strain harden through fewer cycles prior to fatigue failure.

### **6.1.2 AE PARAMETER DATA**

- As the material transitions through stages of crack initiation, crack propagation, and rapid crack growth a graduating growth in event amplitude and duration results.
- Failure regions can be initially separated by evaluation of duration versus amplitude plots and hits versus amplitude histogram plots. Evaluation of the hits versus amplitude plots reveals normal distributions which identify separate modes of failure.
- Duration versus amplitude plots reveal separate modes of failure by correlating with time of occurrence.
- Each material has characteristic regions on the hits versus amplitude plots for its failure modes.
- Overlapping of regions require the application of neural network analysis to separate failure mechanisms.
- AE can be an effective real-time method for determining the time of occurrence of specified failure modes when used in conjunction with a comparison set of AE test parameters.

### **6.1.3 NEURAL NETWORKS AND MULTIPLE LINEAR REGRESSION**

- After evaluation of each distribution set, it was concluded the 250 hit amplitude distributions were most effective for prediction. This size distribution tended to contain data which offered sufficient trends for a neural network to train upon while offering data which mainly consisted of a single failure mechanism, plastic deformation.
- Neural networks require at least two hidden layers to accurately model the nonlinearity that occurs in metal-bellows samples. Nickel alloys have required a larger number of neurons per hidden layer, as opposed to stainless steels, which is probably due to the more complex material composition and crack behavior during material fatigue.
- A neural network can be better developed by updating the network model. With each new set of collected data, the network model can be improved by incorporating the new data into training.
- The two 350 stainless steel samples, which failed to meet the error requirements, were found to be tests which fell within the clustered region of the scatterplots. This region represents normal cycle life values for the Inconel 718 samples; however, cycle lives for 350 stainless steel samples tend to be lower than normal within this region. It is questioned as to whether this represents samples which failed prematurely, and if so, what was the influential variable?
- The multiple linear regression model should be re-evaluated if applied to an expanded data set. A determination will need to be made as to which factor(s) contribute to the region separation seen in the scatterplots. If this factor(s) can be determined, an increased data set will likely show a second trend in data that will require a secondary model for the clustered region. An increased data set will also result in more data points falling within the exponential curve region. Therefore, modifications to the existing statistical model may be necessary to better fit the new data curve.

- Due to the small sample size used in this research for each material, it was required to combine all materials to offer a sufficient data set for statistical analysis. It has been determined that a separate model will be required for non-heat treated materials due to the increase in ductility and longer cycle life which occurs. If large sample sizes can be produced for each material, a better prediction model can likely be developed for each material. Developed models will likely have similar curvature with some variation characterized by an offset.

## **6.2 RECOMMENDATIONS**

To better develop a neural network and statistical model which can accurately predict on new data sets, several modifications will need to be incorporated into any future testing:

- Test samples must be obtained from various material lots and stamping runs. This allows for a larger range of variations within the test samples. Any variations of significance to the cycle life prediction will likely be identified by the neural network and weighted accordingly during the training phase.
- Testing required cycling the bellows an average of 10 to 15 percent of the total cycle life before the 250 hits required for testing was achieved. Lowering the threshold setting to 40 dB will result in more incoming hits of plastic deformation and “noise” being recorded. Although the data will contain more noise, neural networks have been shown to train better when noise exists within the test data. This lower threshold will also allow for sufficient test data to be collected within less than 5 percent of the total cycle life. It may then be possible to use a 500 or 1000 hit distribution if sufficient incoming hits are recorded. This would likely improve the prediction capability of the network.
- Since metal bellows are manufactured in a variety of sizes, but similar in configuration, it may be warranted to incorporate a variety of sizes to determine if prediction can be made on all sizes for a specific material type or whether a separate network is required for each size or range of sizes.

- A larger set of test samples should be used for the training and testing phases. Seven samples were sufficient for a preliminary evaluation, but not enough to implement a secondary validation group to confirm that the designed network will be a good predictor. It is likely, for network training and statistical analysis, a minimum of 30 samples would be needed to create a highly accurate model for prediction. Statistical methods generally require a sample model of at least 30 to be considered an accurate representation of the distribution found in the population model.

## REFERENCES

1. Hill, E.v.K., "Predicting Burst Pressures in Filament-Wound Composite Pressure Vessels by using Acoustic Emission Data," *Materials Evaluation*, Vol. 50, No. 12, Dec. 1992, pp. 1439-1445.
2. Hill, E.v.K., P.L. Israel, and G.L. Knotts, "Neural Network Prediction of Aluminum-Lithium Weld Strengths from Acoustic Emission Data," *Materials Evaluation*, Vol. 51, No. 9, Sep. 1993, pp. 1040-1045, 1051.
3. Kalloo, F.R., "Predicting Burst Pressures in Filament Wound Composite Pressure Vessels Using Acoustic Emission," MSAE Thesis, 1998, Embry-Riddle Aeronautical University, Daytona Beach, FL.
4. Mitchell, J.R., "Testing for Flaws in Reinforced Plastics by Acoustic Emission," *Plastics Engineering*, Jan. 1984, pp. 29-32.
5. Pollock, A.A., "Acoustic Emission Amplitude Distributions," *International Advances in Nondestructive Testing*, Vol. 7, 1981, pp. 215-239.
6. Sachse, W. and I. Grabec, "Intelligent Processing of Acoustic Emission Signals," *Materials Evaluation*, Vol. 50, No. 7, 1992, pp. 826-834.
7. Smith, W., *Foundations of Materials Science and Engineering*, McGraw-Hill, Inc., 1993, pp. 257-262.
8. Tennant-Smith, J., *BASIC Statistics*, Butterworth & Co. Ltd., London, UK, 1985, p. 106.
9. Walker, J.L. and Hill, E.v.K., "An Introduction to Neural Networks: A Tutorial," presented at the First International Conference on Nonlinear Problems in Aviation and Aerospace, Daytona Beach, FL, May 1996, pp. 667-672.
10. Walpole, R., Myers, R., and Myers, S., *Probability and Statistics for Engineers and Scientists*, Prentice Hall, Inc., 1998, pp. 387, 396-397, 428.
11. Walpole, R. and Myers, R., *Probability and Statistics for Engineers and Scientists*, Prentice Hall, Inc., 1993, pp. 456-457.
12. Wasserman, P.D., *Neural Computing: Theory and Practice*, Van Nostrand Reinhold, New York, NY, 1989, pp. 15-16, 19.

## BIBLIOGRAPHY

1. NeuralWare, Inc., *Reference Guide NeuralWorks Professional II/Plus and NeuralWorks Explorer*, 1995.